4-15-2019

Evaluating a new algorithm for satellite-based evapotranspiration for North American ecosystems: Model development and validation

Bassil El Masri

Abdullah F. Rahman
The University of Texas Rio Grande Valley

Danilo Dragoni

Recommended Citation

El Masri, Bassil, Abdullah F. Rahman, and Danilo Dragoni. "Evaluating a new algorithm for satellite-based evapotranspiration for North American ecosystems: Model development and validation." Agricultural and forest meteorology 268 (2019): 234-248. https://doi.org/10.1016/j.agrformet.2019.01.025

Evaluating a New Algorithm for Satellite-based Evapotranspiration for North American Ecosystems: Model development and Validation

Authors: Bassil El Masri [1*], Abdullah F. Rahman [2], and Danilo Dragoni[3]

[1] Department of Earth and Environmental Sciences, Murray State University, Murray State University, KY, 42071.

[*] Corresponding author: Tel: 270-809-3110

[2] School of Earth, Environmental, and Marine Sciences, University of Texas Rio Grande Valley, Brownsville, TX, 78520

[3]Nevada Division of Environmental Protection, Carson City, NV, 89701

Email addresses: belmasri@murraystate.edu (B. El Masri), abdullah.rahman@utrgv.edu (A.F. Rahman), ddragoni@ndep.nv.gov (D. Dragoni).

Abstract

We introduce "a different operational approach" to estimate 8-day average daily evapotranspiration (ET) using both routinely available data and the Penman-Monteith (P-M) equation for canopy transpiration and evaporation of intercepted water and Priestley and Taylor for soil evaporation. Our algorithm considered the environmental constraints on canopy resistance and ET by (1) including vapor pressure deficit (VPD), incoming solar radiation, soil moisture, and temperature constraints on stomatal conductance; (2) using leaf area index (LAI) to scale from the leaf to canopy conductance; and (3) calculating canopy resistance as a function of environmental variables such as net radiation and VPD. Remote sensing data from the Moderate Resolution Spectroradiometer (MODIS) and satellite soil moisture data were used to derive the ET model. The algorithm was calibrated and evaluated using measured ET data from 20 AmeriFlux Eddy covariance flux sites for the period of 2003-2012. We found good agreements between our 8-day ET estimates and observations with mean absolute error (MAE) ranges from 0.17 mm/day to 0.94 mm/day compared with MAE ranging from 0.28 mm/day to 1.50 mm/day for MODIS ET. Compared to MODIS ET, our proposed algorithm has higher correlations and higher Willmott's index of agreement with observations for the majority of the Ameriflux sites. The strong relationship between the model estimated ET and the flux tower observations implies that our model has the potential to be applied to different ecosystems and at different temporal scales.

Keywords:

Penman-Monteith; Evapotranspiration; MODIS; Remote sensing; Eddy covariance flux.

1 Introduction

Estimating evapotranspiration (ET) is important for water and land resources management because it "is an essential component of the water and energy cycles". It is vital for climate change models "because ET is sensitive to changes in surface albedo [Mattar et al., 2014] and it can play an important role in driving local weather conditions including air temperature and precipitation [Fisher et al., 2017]". ET estimates are important for understanding and modeling terrestrial ecosystem productivity because ET is related to the energy transferred between the terrestrial ecosystem and the atmosphere. The connection between ET and terrestrial ecosystem productivity is due to the strong relationship between stomatal conductance, which controls the rate of water, and carbon exchange between the atmosphere and vegetation [Beer at al., 2007, 2009; Farquhar and Sharkey, 1982; Wong et al., 1979], and the rate of carbon assimilation [Chaves, 1991; Goulden, 1996; Law et al., 2002; Medrano et al., 2002; Schulze et al., 1994]. Improving the accuracy as well as the spatial and temporal coverage of ET estimates will reduce the uncertainty in the water budget and will provide valuable information for applications requiring ET estimates.

Several methods for estimating ET were developed that ranged from point estimates to complex land surface models [Bastiaanssen et al., 1998a; Cleugh et al., 2007; Su et al., 2005]. Yet, the applicability of these approaches is dependent on the availability of the required input parameters "hinders" their application globally. Satellite remote sensing is a promising tool for scaling measurements from the local to the regional and global scales. It provides continuous spatial and temporal information about surface parameters such as albedo and emissivity that can be used for ET estimation. For instance, the Moderate Resolution Imaging Spectroradiometer (MODIS) provides data twice a day that are crucial for model developments aimed at remote monitoring of terrestrial ecosystem evapotranspiration.

Over the last decade, several methods were developed to estimate ET from satellite data. These methods can be categorized into three groups: (1) triangle methods (Vegetation indices- surface temperature (T_s) [Jiang et al., 2009; Jiang and Islam, 2001; Long and Singh, 2012; Merlin et al., 2014; Nemani and Running, 1989; Nishida et al., 2003; Yang and Shang, 2013], (2) energy balance models "using" satellite-observed land surface temperature to compute the components of the surface energy budget [Bastiaanssen et al., 1998a, 1998b; Kustas and Norman, 1999; Long and Singh, 2012; McVicar and Jupp, 1999, 2002; Norman et al.,1995; Su, 2002], and (3) "remote-sensing-only" driven ET using the Penman-Monteith or the Priestley and Taylor methods [Cleugh et al., 2007; Fisher et al., 2008; García et al., 2013; Miralles et al., 2011; Mu et al., 2007, 2011; Leuning et al., 2008; Zhang et al., 2008]. Intensive intercomparison studies have been conducted to compare and evaluate ET models driven only by satellite data [Ershadi et al., 2014; McCabe et al., 2016; Miralles et al., 2016; Michel et al., 2016; Vinukollu et al., 2011]. Results of these studies showed that all approaches performed well with discrepancy that can be traced back to differences in the models schemes. In general, models did not outperform one another [McCabe et al., 2016] and all overestimated observed ET for dry sites where ET is limited by soil moisture availability [Michel et al., 2016].

"However, these remote sensing driven ET models estimates varies drastically with the choice of climate reanalysis data (Mu et al., 2007, 2011; Yao et al., 2017) due to biases in these datasets. Thus, minimizing or eliminating the need for inputs from climate reanalysis data can increase the accuracy of remote-sensing-only driven ET models. In addition, majority of remote-sensing-only driven ET models rely on meteorological forcing to account for soil moisture limitation on ET instead of satellite land surface temperature and may lead to slower ET response to soil moisture changes [Long and Singh, 2010]. Hence, remote sensing ET models should use satellite land surface temperature to account for soil moisture restriction on ET [Yang et al., 2015]."

In this study, we utilized the Penman-Monteith method (hereafter P-M) for canopy transpiration and the Priestly and Taylor (hereafter P-T) methods for soil evaporation estimation using optical and thermal data from the MODIS and fusion of data from multiple sensors. We built up on existing approaches to develop our ET model through the combination of different satellite data sources and different methods to estimate the required meteorological inputs from satellite observations. Key distinguishing feature from other satellite based P-M approaches is the use of a single global parametrization for stomatal conductance instead of biome specific relationships to maximum stomatal conductance [Mu et al., 2007, 2011; Zhang et al., 2016] and vapor pressure deficit (VPD) based on MODIS surface temperature instead of VPD from coarse spatial resolution climate reanalysis data [Zhang et al., 2010]. We also demonstrated here that combining previously established methods into one model can be applied to estimate ET using solely satellite observations.

The objective of this study was to develop and evaluate a model for monitoring terrestrial ecosystem evapotranspiration using satellite data only. Our goal was to eliminate the need for climatic reanalysis data by incorporating optical, thermal, and microwave remote sensing information to estimate the required model inputs, such as vapor pressure deficit. Model performance was compared and validated with field data from 20 Ameriflux Eddy Covariance flux towers sites representative of the major North American biomes. Uncertainties and error analysis were computed for the model outputs. Finally, the model results were compared with MODIS evapotranspiration product (hereafter referred as MOD16) to demonstrate that the model results present an improvement compared to MOD16.

2 Methods

2.1 ET algorithm

We proposed a fundamentally different operational approach to develop a remote sensing data driven process-based method for estimating ET that uses the P-M equation for canopy evaporation and transpiration and P-T equation for soil evaporation (hereafter called RS-PMPT). In our approach we did not alter the P-M or P-T equation. Instead, we estimated each of their parameters using only satellite data in order to gain insight about the ability of available remotely sensed data to derive P-M and P-T equations (Fig. 1)

The Penman-Monteith [Monteith, 1965] estimate evapotranspiration as:

$$\lambda E = \frac{s(R_n - G) + (\rho C_p \frac{VPD}{r_a})}{s + \gamma(1 + \frac{r_c}{r_a})} \qquad 1$$

where λE is the latent heat flux (W/m^2), λ is the latent heat of vaporization (J/kg), s is the slope of the curve relating saturated water vapor pressure to temperature (kPa), R_n is the net solar radiation (W/m^2), G is soil heat flux (W/m^2), ρ is air density (kg/m^3), C_p is specific heat capacity of air (J/kg/K), VPD is vapor pressure deficit (kPa), r_a is the aerodynamic resistance (s/m), γ is the Psychrometric constant (kPa/K), and r_c is the canopy resistance (s/m) for evaporation from the leaves and transpiration from the plant canopy.

In the RS-PMPT model fraction of the photosynthetically active radiation (fpar) is used as surrogate for vegetation cover fraction [Mu et al., 2011] to partition net radiation (R_n) between the canopy and the soil:

$$R_{nc} = R_n \times fpar \tag{2}$$

$$R_{ns} = (1 - fpar) \times R_n \tag{3}$$

where R_{nc} is the canopy net radiation, R_{ns} is soil net radiation, and $fpar$ is the fraction of photosynthetically active radiation from MODIS. In the RS-PMPT model, plant evapotranspiration is the sum of canopy transpiration and evaporation of intercepted water by the canopy. The relative surface wetness (f_{wet}) is used to determine whether the surface is wet or not following Fisher et al. [2008] with modification by Mu et al., [2011] and Yao et al. [2013]:

$$f_{wet} = \begin{cases} 0 & RH < 70\% \\ fsm^4 & 70\% \leq RH \leq 100\% \end{cases} \tag{4}$$

where RH (%) is daily mean RH estimated from midday MODIS land surface temperature (LST) and daily mean MODIS LST. RH is calculated as $(e_a \times 100)/e_s$, "where e_s is saturated vapor pressure at T_S estimated following Running and Coughlan [1988]:"

$$e_s(Pa) = 6.1078 e^{\frac{17.269 T_S}{237.3 + T_S}} \tag{5}$$

e_a is actual vapor pressure estimated using equation 5, but by replacing daytime LST with average day and night LST. Soil moisture constraint is estimated as:

$$\boldsymbol{fsm = \left(1/_{DT}\right)^{DT/_{DT_{max}}}} \tag{6}$$

where DT= LST_{day} –LST_{night} and DT_{max} = 60 °C [Yao et al., 2013]. f_{wet} is used to determine when to estimate evaporation from wet canopy and from wet soil surface.

2.1.1. Plant Transpiration

MODIS daytime land surface temperature (T_S) data were used in the algorithm because recent studies showed that T_S can be used as reliable estimator of air humidity, specifically e_s

[Granger, 2000; Hashimoto et al., 2008]. The curve relating e_s and T_S was used to derive s, VPD is estimated based on the approach of Hashimoto et al. [2008; Fig. 5] that related e_s (equation 5) to VPD as:

$$VPD = 0.391 \times e_s - 0.028 \tag{7}$$

Canopy resistance (r_c:s/m) was found to vary with different environmental variables. For instance, canopy resistance decreases with an increase in temperature and VPD [Jarvis, 1976]. Following Stewart [1988], r_c was modeled as a product of the response functions to different environmental variables that acts independently on r_c (see Damour et al. 2010 for more detailed assumptions about the multiplicative models of canopy resistance). The Stewart [1988] r_c model is based on Jarvis's model [Jarvis, 1976] with modified environmental constraints. This approach was tested successfully at different biomes [Dingman, 2002; Stewart, 1988; Stewart and Gay, 1989] and model parameters were fitted using multivariate optimization technique. r_c is calculated as:

$$r_c = \frac{1}{f(T_s) \times f(\theta) \times LAI \times f(VPD) \times f(R_s) \times 0.5 \times C_{leaf}} \tag{8}$$

where, $f(T_S)$ is the temperature multiplier, $f(VPD)$ is the VPD multiplier, $f(\theta)$ leaf water content deficit multiplier, $f(R_s)$ is the solar radiation multiplier, C_{leaf} is the maximum leaf conductance set to 5.3×10^{-3} ms^{-1}, which is the typical value for forest, shrub, and Savannah ecosystems [Dingman, 2002; Schulz et al., 1994], 0.5 is a shelter factor that accounts for the fact that some leaves are shaded from the sun and have a minimum contact with wind, thus transpire at a lower rate [Dingman, 2002]. The shelter value was used as only one half of the leaf area in vegetated areas are effective in ET and a value of 0.5 is probably a good estimate for a dense vegetated area [Allen et al., 1989]. Stewart [1988] tested the sensitivity of environmental multiplier to ±20 % change in their parameters values and found that temperature and vapor pressure deficits functions were highly sensitive to changes in their parameters values, while solar radiation and soil moisture functions had very little sensitivity. Based on this finding, only parameters values for temperature and vapor pressure deficit functions were calibrated (see below). We calculated the constraints on stomatal conductance for temperature [Gerosa et al., 2012] and VPD [Mu et al., 2007] as:

$$f(T_s) = \begin{cases} 1 & T_s = T_{opt} \\ \dfrac{(T_s - T_{\min})}{(T_{opt} - T_{\min})} \times \left[\dfrac{(T_{max} - T_s)}{(T_{max} - T_{opt})}\right]^{\left(\frac{T_{max} - T_{opt}}{T_{opt} - T_{min}}\right)} & T_{min} \leq T_s \leq T_{opt} \\ 0.1 & T_s \leq T_{min}\ or\ T_s \geq T_{max} \end{cases} \tag{9}$$

$$f(VPD) = \begin{cases} 1 & VPD \leq VPD_{open} \\ \dfrac{VPD_{close} - VPD}{VPD_{close} - VPD_{open}} & VPD_{open} < VPD < VPD_{close} \\ 0.1 & VPD \geq VPD_{close} \end{cases} \tag{10}$$

Where T_{opt} is the optimal temperature equal to 25 °C, T_{min} is minimum temperature equal to 0 °C, T_{max} is the maximum temperature equal to 50 °C and VPD_{close} indicates stomatal inhibition due to high VPD and is set to 2.5 KPa based on flux tower observations for the forest sites and 4 KPa for grassland and savannah sites. VPD_{open} indicates no inhibition to transpiration and is set to 0.4 KPa for the forest, grassland and savannah sites. "When T_S is lower or higher than the T_S threshold (T_{min}, T_{max}) or VPD is higher than VPD_{close}, stomatal will close halting plant transpiration because of temperature or VPD stress. Similarly, when Ts is equal to T_{opt} and VPD is less than or equal to VPD_{open}, stomatal is open and plant transpiration is not limited by temperature or VPD stress. The multipliers range from 0 for total inhibition on stomatal conductance to 1.0, which means there is no inhibition by VPD and T_s on stomatal conductance". The parameters (VPD_{close}, VPD_{open}, T_{max}, T_{opt}, and T_{min})

used for in equations 8 and 9, which have strong effect on ET simulation were calibrated by direct comparison of observed and modeled ET. We optimized the model outcome by using trail and error method, which found the calibrated parameters values for VPD_{close}, VPD_{open}, T_{max}, T_{opt}, and T_{min} that could achieve the minimum difference between "the 8-day" modeled ET and "the 8-day Ameriflux" ET for the "calibration" sites. Since VPD_{close} parameters varies between "forested and non-forested areas", the optimization is done for forest calibration sites and savannah and grassland calibration sites, "independently". Leaf water content represents the effect of soil moisture deficit in leaf conductance that influences transpiration rates. Leaf water content (cm) is calculated according to Dingman [2002] following Stewart [1988]:

$$f(\theta) = 1 - 0.00119 \times e^{(0.81 \times \Delta SM)} \qquad 11$$

where ΔSM (m^3/m^3) is the soil moisture deficit defined as the max (SM for the growing season) – SM_d, where "SM_d is the soil moisture for a given" day of the year. Incident solar radiation constraint is estimated following Dingman [2002] and Stewart [1988]:

$$f(R_s) = \frac{12.78 \times R_s}{11.57 \times R_s + 104.4} \qquad 12$$

where R_s is the incoming shortwave radiation (Wm^{-2}).

r_a (s/m) is estimated according to the following equation:

$$r_a = 0.012 \times \rho \times C_p \qquad 13$$

where 0.012 is the mean net radiation coefficient from the multiple regression between temperature and multiple environmental variables for different ecosystem types [Thornton, 1998], ρ is the air density, and C_p is the specific heat capacity of air.

Air density (ρ) is calculated using the ideal gas law and expressed as a function of atmospheric pressure and MODIS LST:

$$\rho\ (kgm^{-3}) = \frac{P}{R \times T_s} \tag{14}$$

where P is the atmospheric pressure (Pa), R is the specific gas constant set to 287.05 $Jkg^{-1}K^{-1}$. P is calculated with respect to the elevation of each site:

$$P = P_0 \times \left[\frac{T_b}{T_b + L_b \times (h - h_b)}\right]^{\frac{g \times M}{R \times -L_b}} \tag{15}$$

where P_0 is the standard sea level atmospheric pressure = 101325 Pa, L_b is the temperature lapse rate = 0.0065 Km^{-1}, h-h_b is the altitude (m), T_b is the sea level standard temperature = 288.15 K, R is the universal gas constant = 8.314 472(15) $Jmol^{-1}K^{-1}$, M is the molar mass of the earth of Earth's air = 0.0289644 kg/mol, and g is the earth-surface gravitational acceleration = 9.80665 ms^{-2}. We used surface temperature because studies showed a strong relationship between MODIS LST and air temperature [Mildrexler et al., 2011; Yang et al., 2017] and because our purpose was not to use climate reanalysis data.

Finally, plant transpiration is calculated as:

$$\lambda E_c = \frac{\left[s \times R_{nc} + \left(\rho \times C_p \frac{VPD}{r_a}\right)\right] \times (1 - f_{wet})}{s + \gamma(1 + \frac{r_s}{r_a})} \tag{16}$$

2.1.2. Wet canopy evaporation

Studies have showed that evaporation from water intercepted by the canopy was a significant contributor toward total ET from dense canopy [Grimmond et al., 2000]. When the canopy is wet, mostly evaporation of intercepted water will occur. For wet canopies, several studies have shown that r_c is negligible [Stewart, 1977; Van der Tol et al., 2003]. The evaporation for wet canopy surface is calculated as:

$$\boldsymbol{\lambda E_{c\_wet}} = \frac{\left[\boldsymbol{s} \times \boldsymbol{R_{nc}} + \left(\boldsymbol{\rho} \times \boldsymbol{C_p} \times \frac{\boldsymbol{VPD}}{\boldsymbol{r_a}}\right)\right] \times \boldsymbol{f_{wet}}}{\boldsymbol{s} + \frac{\boldsymbol{C_p} \times \boldsymbol{P}}{\boldsymbol{\lambda} \times \boldsymbol{M} \times \boldsymbol{r_a}}} \quad 17$$

where M is the ratio of molecular weight of water vapor to dry air (M= 0.622).

2.1.3 Soil Evaporation

The Priestley and Taylor (1972) equation for potential ET is used to calculate soil evaporation [Fisher et al., 2008] in the RS-PMPT model and is constrained by soil moisture limitation (f_{SM}) on soil evaporation that is used to reduce potential ET to actual ET:

$$\boldsymbol{\lambda E_s} = [\boldsymbol{f_{wet}} + \boldsymbol{f_{SM}} \times (\boldsymbol{1} - \boldsymbol{f_{wet}})] \times \boldsymbol{\alpha} \frac{\boldsymbol{s}}{\boldsymbol{s} + \boldsymbol{\gamma}} (\boldsymbol{R_{ns}} - \boldsymbol{G}) \quad 18$$

Where α = 1.26 is Priestley and Taylor coefficient, R_{ns} is net radiation to the soil, and G is ground heat flux. Soil moisture constraint is calculated following Verstraeten et al. [2006]:

$$f_{SM} = \left(\frac{ATI - ATI_{min}}{ATI_{max} - ATI_{min}}\right) \quad 19$$

Where ATI is the apparent thermal inertia index [Garcia et al. 2013] and calculated as:

$$ATI = C \frac{1 - a}{T_{S_{max}} - T_{S_{min}}} \quad 20$$

$$C = sin\alpha sin\delta \times (1 - tan^2\alpha \times tan^2\delta) + cos\alpha \times cos\delta \times \arccos(-tan\alpha \times tan\delta) \quad 21$$

Where $T_{S_{max}}$ is maximum daytime T_S, $T_{S_{min}}$ is minimum nighttime T_S, a is MODIS albedo, α is latitude and δ is solar declination estimated used the method of Iqbal [1983], and ATI_{min} and ATI_{max} are the seasonal minimum ATI and maximum ATI, respectively. We noted that maximum T_S was calculated as the mean of daytime MODIS LST Terra and Aqua satellites data, whereas minimum T_S is calculated as the mean of nighttime MODIS LST Terra and

Aqua satellite data.

Ground heat flux is calculated as a function of LAI and R_n following Kustas et al., [1993] as:

$$G = 0.4 \exp(-0.5 \times LAI) \times R_n \qquad 22$$

The above equation estimates G = 0.1R_n for LAI = 2.8 and G = 0.4R_n for LAI = 0. Net radiation to the soil was partitioned from R_n using MODIS fpar (see equation 3).

2.1.4 Total Daily ET

The daytime total ET is the sum of the canopy transpiration and evaporation from intercepted water if the canopy is considered wet based on RH and soil evaporation. Total ET is calculated as:

$$ET\ (\frac{mm}{day}) = (\frac{\lambda E_c}{\lambda} + \frac{\lambda E_{c_{wet}}}{\lambda} + \frac{\lambda E_s}{\lambda}) \times dl \qquad 23$$

Where dl is day length. Daytime length (dl) is estimated based on Hunt et al. [1996]:

$$dl\ (\text{sec}) = 480 \times cos^{-1}(-tan\theta \times tand_s) \qquad 24$$

Where θ is the latitude in degrees, and d_s is the sun declination in degrees.

The approaches used in the RS-PMPT model to estimate stomatal conductance and surface wetness have been tested and applied to different vegetation types, and climate resulting in accurate ET estimation when compared to site observations [Fisher et al., 2008; Gerosa et al., 2013; Jarvis, 1976; Muo et al., 2011; Stewart, 1988; Stewart and Gay, 1989; Zhang et al., 2010]. The scientific basis for these approaches was introduced first by Jarvis [1976] by measuring the response of stomatal conductance against environmental data, modified by Stewart [1988] and have been discussed in the literature cited above. Estimating ET using only satellite data required the use of approaches that could be modified to run with remote sensing data and eliminated the use of local or derived meteorological data. For instance, to estimate VPD using remote sensing data the approach of Hashimoto et al. [2008] was used (Table 1).

2.2 Data

2.2.1 Flux Tower Data

We calibrated and validated the model across a wide range of ecosystem types and climate at 20 AmeriFlux flux sites for years 2003-2012 (Table 2). Flux data sets provide several environmental and ecosystem functions variables [Baldocchi et al., 2001] and were used for the calibration and validation of the model. We acquired gap-filled flux data (FLUXNET2015) from the AmeriFlux website (https://ameriflux.lbl.gov/). Marginal distribution sampling method was used to gap-fill the flux data [http://fluxnet.fluxdata.org/data/fluxnet2015-dataset/]. To calculate daily daytime LE_d (Jm^{-2}) from half-hourly data, we defined day length as the period with photosynthetically active radiation (PAR) greater than 15 $\mu molm^{-2}s^{-1}$. Then, daily daytime tower LE_d (Jm^{-2}) was calculated as the sum of the day length half hourly LE data as $LE_d = (\sum_i^n LE) \times 60 \times 30$. The tower measured daily daytime ET is calculated from daily daytime LE_d as:

$$ET_d = \frac{LE_d}{\lambda} \qquad 25$$

where d is total observation of each day, and λ is the latent heat of vaporization (Jkg^{-1}). λ is calculated based on Maidment [1993] equation:

$$\boldsymbol{\lambda\ (\mathrm{JKg^{-1}}) = (2.501 - 2.36 \times 10^{-3} \times \mathrm{T_S}) \times 10^{6}} \qquad 26$$

Furthermore, 8-day mean ET (Tower ET) is calculated as the average of 8-day ET for the days that were considered cloud free (days with average PAR values greater than 400 $\mu molm^{-2}s^{-1}$). We did not calculate the 8-day ET average if three or more days were missing data. The 8-day average for ET was computed to match the temporal resolution of MODIS evapotranspiration product.

2.2.2 Satellite data

"Detailed information about satellite data version, layers, and layers names are provided in Table 1". Leaf area Index [Myneni et al., 2015], fraction of photosynthetically active radiation [Myneni et al., 2015], MODIS land surface temperature LST [Wan et al., 2015], and calculated albedo (MCD43A) [Schaaf and Wang, 2015] were obtained from the 7 × 7 km subsets of MODIS products (1 km spatial resolution; "version 005) using the MODIS Web Service Tool [ORNL DAAC, 2008] (https://modis.ornl.gov/data/modis_webservice.html)". Although the flux tower footprint is about 1 km^2 [Schmid, 2002], exactly locating the pixel where the flux tower footprint falls within can be a difficult task. Therefore, we extracted the central 3 × 3 km area within the 7 × 7 km subsets. Above-mentioned data came from the Terra and Aqua satellites and the average of Terra and Aqua data was used to run the RS-PMPT model. "We used data from either Terra or Aqua for days when Terra or Aqua data were missing due to quality control. Albedo was calculated as the average of the shortwave black sky albedo and shortwave white sky albedo". Soil moisture data (25 km spatial resolution) were downloaded from European space agency website (http://www.esa-soilmoisture-cci.org/node/215). Soil moisture data (CCI SM v03.2) is available daily and produced from the fusion of multiple sensors [Dorrigo et al., 2017]. Satellite daily solar radiation data (1° spatial resolution) were downloaded from NASA "Cloud and the Earth's Radiant Energy System (CERES)" website (https://ceres.larc.nasa.gov/products.php?product=SYN1deg) [Smith et al., 2011; Wielicki et al., 1996]. CERES (SYN1deg-Day, edition 3) provides computed fluxes for incoming shortwave and longwave radiations (1° spatial resolution) and outgoing shortwave and longwave radiation (1° spatial resolution) and has been extensively evaluated [Doelling et al., 2013]. CERES data were used to calculate R_n.as the difference between the incoming and the outgoing radiation. MODIS evapotranspiration (MOD16A2; variable name: ET_1km) [Running et al., 2017] data were obtained from the 3 × 3 km subsets of MODIS product "(version 005) using the MODIS Web Service Tool [ORNL DAAC, 2008] (https://modis.ornl.gov/data/modis_webservice.html)". Periods with missing data were not filled. Only data with high quality control for LAI and *f*par were used. LAI and *f*par high quality control (000 and 001; see MODIS Collection 5: LAI/fPAR Product User's Guide: "https://lpdaac.usgs.gov/sites/default/files/public/modis/docs/MODIS-LAI-FPAR-User-Guide.pdf") indicated than the main radiation transfer (RT) algorithm was used. LAI and *f*par data quality control allowed for the identification of LAI and *f*par values produced with the backup algorithm that are considered the least reliable [Yang et al., 2006] and these LAI and *f*par values were replaced with values generated from linear interpolation. For days where linear interpolation could not be used because of multiple consecutive missing 8-day data, the day was dismissed from the analysis and we could not compute the RS-PMPT ET for that 8-day period. In general, less than 9% of the LAI and *f*par data for some sites (e.g. Duke Forest) required linear interpolation due to low quality data. We used LAI and *f*par data from either Terra or Aqua when data from one of these satellites were missing. In case no LAI or *f*par data were available from MODIS, gap-filling was not used for that day because usually other MODIS data were missing such as, albedo and LST.

2.3 Statistical analysis

Two levels of error analysis for the proposed model outputs were computed. First, the model derived ET was validated with ET obtained from eddy flux tower measurements and MOD16. Coefficient of determination (r^2), root mean square error (RMSE), mean absolute error (MAE) were used to validate the RS-PMPT ET results. Second, Willmott's index of agreement (d) was used to quantify the model results. In this paper, RMSE is defined as the difference between two data sets for all samples and it is given by:

$$RMSE = \frac{1}{n}\sum_{i=1}^{n}(X_i - Y_i)^2 \tag{27}$$

where X_i is the observed value and Y_i is the estimated value. Mean absolute error (MAE) is defined as the absolute difference between the two data sets for all samples and it is given by:

$$MAE = \frac{1}{n}\sum\nolimits_{i=1}^{n} abs(X_i - Y_i) \tag{28}$$

Willmott's index of agreement (*d*) [1981, 1982, 2011] is defined as:

$$d = 1 - \frac{\sum_{i=1}^{n}(X_i - Y_i)^2}{\sum_{i=1}^{n}(|X_i - \bar{X}| + |Y_i - \bar{X}|)^2} \tag{29}$$

where $\bar{X}$ is the mean of the observed value. Willmott's index varies between -1 and 1, a value of 1 means that the two data sets are in perfect agreement and a d of −1 indicates either lack of agreement between the model and observation or insufficient variation in observations to adequately test the model. The ability of Willmott's index of agreement to measure the model errors makes it use appropriate for model validation. Willmott's index of agreement can measure two sources of errors: systematic and unsystematic errors. Unsystematic errors quantify model precision, while systematic error refers to the linear bias produced by the model. Applying and building the appropriate regression functions can reduce the systematic error.

Willmott's defined the systematic mean square error (MSE_s) as:

$$MSE_s = \frac{1}{n}\sum\nolimits_{i}^{n}(X_{i -} \hat{Y}_i)^2 \tag{30}$$

where X_i is the observed value, $\hat{Y}$ is the predicted Y obtained from the regression equation model $\hat{Y} = a + bX$. The unsystematic mean square error (MSE_{us}) is defined as:

$$MSE_{us} = \frac{1}{n}\sum_{i}^{n}(Y_i - \hat{Y}_i)^2 \tag{31}$$

where Y_i is the estimated value. The proportion of the systematic error and unsystematic errors to the total errors was derived from MSE_s / MSE and MSE_{us}/ MSE, respectively. MSE is the sum of MSE_s and MSE_{us}.

3 Results

3.1 Model results for the calibration sites

The RS-PMPT estimates were compared to the tower ET. To test the overall seasonal prediction of the RS-PMPT model, an 8-day growing season mean for the study sites were generated. We used either Terra or Aqua data for days with data available only from one of these two sensors; otherwise data from both sensors were averaged and used for the model inputs. For the deciduous sites, the RS-PMPT model could track successfully the seasonal variation of the tower ET (Fig. 2). The RS-PMPT model underestimated the peak tower ET for MMSF (except for years 2004 and 2008). The underestimation could be due to errors in the model satellite inputs or model parameters ($VPDo_{pen}$, VPD_{close}, etc.) that were used to estimate r_c.

For the evergreen sites, the RS-PMPT model was in good agreement with the tower ET (Fig. 3). The RS-PMPT overestimated tower ET for the subtropical evergreen forest (Austin Cary) before Julian day 120, but was able to track the seasonality of tower ET for the rest of the year (Fig. 3). Comparison of site measured LAI and MODIS LAI revealed that the later overestimate the former by about $1 m^2 m^{-2}$ (data not shown) for Austin Cary before Julian day 120. Thus, errors in MODIS LAI have contributed to the observed ET overestimation by RS-PMPT.

The RS-PMPT model was able to track the seasonal variability in the tower ET for the grassland sites and the woody savanna site (Figs. 4 & 5). The RS-PMPT model underestimated the peak ET for year 2004 for the Lethbridge site and overestimated the end of the growing season ET for Vaira Ranch (Fig. 4). The model performed poorly for the shrubland site, which can be attributed to low MODIS LAI (< 1 m^2/m^2), but it was able to track the seasonal variability in the tower ET for the savanna site (Fig. 5).

Regression analysis was performed by averaging the 8-day means of tower ET for each of the study sites. The results showed strong and significant correlation between the RS-PMPT model and tower for all the calibration sites (Fig. 6). The r^2 ranged from 0.38-0.97, with the lowest r^2 for Sky Oaks (r^2 = 0.38) site mainly due to the underestimation discussed above "and in the discussion section". Whereas, MOD16 r^2 ranged from 0.06-0.96 with an average r^2 of 0.72 compared with an average r^2 of 0.79 for the RS-PMPT (Table 3). The regression analysis results for most of the calibration sites were scattered around the 1:1 line. Low systematic errors (high accuracy) were represented by the plots for the study sites that had estimates close to the 1:1 line and had low $\%MSE_s/MSE$ values, such as US-MMS and Harvard sites (Fig. 6, and Table 3). The proportion of errors for majority of the calibration sites was mainly dominated by unsystematic error, suggesting that the results were unbiased. The proportion of error for Howland forest, Austin Cary, and Lethbridge sites was dominated by systematic error, suggesting that the results may have been biased as the RS-PMT model overestimated or underestimated the peak observed ET for these sites (Table 3). The MAE and RMSE for the RS-PMPT model were much smaller than MOD16 for all the sites, except for the Vaira Ranch site and "ranged for MAE from 0.15 mm/day to 0.57 mm/day" (Table 3). For all the calibration sites, the average MAE for the RS-PMPT and MOD16 was 0.3

mm/day and 0.6 mm/day, respectively; and the average RMSE was 0.42 mm/day and 0.74 mm/day, respectively (Table 3). The high value of *d* for the RS-PMPT model is an indication of the good agreement between the modeled ET and the tower ET (Table 3). The *d* values for the RS-PMPT model were much closer to one than MOD16, except for the Vaira Ranch site (Table 3).

3.2 Model results for the validation sites

Validation of the model was performed for four deciduous sites, two evergreen sites, and 6 grassland sites. The RS-PMPT model estimates were evaluated and compared with site flux tower ET. RS-PMPT estimates were able to track the seasonal variability in the deciduous, evergreen, and grasslands sites, suggesting that the RS-PMPT model can be applied successfully to other sites (Figs 7-9). This was also supported by the high d values (Table 3). In general, the intra and interannual variability in the tower ET was detected by the RS-PMPT model.

For the deciduous sites and evergreen sites (Figs.7-8), the RS-PMPT was able to track accurately the interannual the seasonality in the observed ET. The ET underestimation for US-DK3 site could be related to the use of maximum stomatal conductance that is not representative of this site leading to overestimation of surface resistance (Fig 8.). For the US-Bkg grassland site, the model underestimated flux tower ET (Fig.9). It is important to note that US-Bkg is a managed grazed pasture site and management practices probably contributed to the mismatch between RS-PMPT estimated and flux tower ET. For the US-IB2 grassland site, underestimation of the flux tower ET is also observed (Fig. 9).

Regression analysis was performed by averaging the 8-day means of tower ET for each of the validation sites. The results showed strong and significant correlations between the RS-

PMPT model and tower for all the validation sites (Fig. 10). The r^2 ranged from 0.78-0.96, with the lowest r^2 for the US-Bkg ($r^2 = 0.76$) site, while MOD16 r^2 ranged from 0.43-0.97 with an average r^2 for all the validation site of 0.81 compared to an average of r^2 of 0.9 for the RS-PMPT. Low systematic error (MSE_s) was observed for most of the sites (except US-DK3 and US-Kon sites) when compared to MOD16 (Table 3), indicating the high accuracy in RS-PMPT model estimation. The proportion of errors for five of the validation sites was mainly dominated by unsystematic error, suggesting that the results are unbiased. This indicate that our method was able to reduce the biases with observations when compared to MOD16 proportion of error that is mainly dominated by systematic error (Table 3). The MAE and RMSE for the RS-PMPT model were much smaller than MOD16 "(MAE ranges from 0.28 mm/day to 0.81 mm/day; RMSE ranges from 0.4 mm/day to 1.13 mm/day)" for all the sites, except for the CA-Man, US-Bkg, US-IB2, US-Kon and US-DK3 sites "and ranged from 0.17 mm/day to 0.94 mm/day and from 0.21 mm/day to 1.44 mm/day for MAE and RMSE, respectively" (Table 3). MOD16 lower MAE for these sites was due to better estimating the observed ET than the RS-PMPT for certain years (Fig. 8-9). For example, MOD16 was able to replicate the peak of the observed ET for year 2005 for the US-Bkg site, resulting in lower MAE and RMSE than the RS-PMPT (Fig. 9). For the wetter grassland sites (US-Bkg, US-IB2, US-Kon) MOD16 had lower errors than our model, but performed poorly for the semiarid grassland sites (US-Wkg, US-Seg, and US-FPe). Possibly, MOD16 parameters were more representative for the wet grassland sites, whereas the surface wetness model and the use of ATI in determining the soil moisture limitation in the soil evaporation model resulted in more accurate RS-PMPT ET estimates for the semiarid grassland sites (Fig. 9). The high value of *d* for the RS-PMPT model is an indication of the good agreement between the modeled ET and the tower ET (Table 3). The *d* values for the RS-PMPT model were much closer to one than MOD16, except for US-DK3, US-Bkg, and US-IB2 sites (Table 3). For all the validation sites, the average MAE for the RS-PMPT and MOD16 was 0.36 mm/day and 0.47 mm/day, respectively, and the average RMSE was 0.51 mm/day and 0.61 mm/day, respectively (Table 3). The errors and correlation coefficients of the RS-PMPT are very good at the different biome types, indicating that our approach worked well.

4 Discussion

"Overall, the" RS-PMPT model appeared to be robust and applicable for our study sites. This is illustrated in the RS-PMPT ability to track the seasonal variability in the flux tower ET measurements. Hence, its simple parameterization produced results "with RMSE ranging from 0.19 to 0.61 mm/day" similar to the other remote sensing P-M based models [Cleugh et al., 2007; Mu et al., 2007, 2011; Leuning et al., 2008]. The correlation coefficient between the RS-PMPT and observations (Table 3) was very similar to the correlation coefficient of 0.67 and 0.96 for the study sites [Lu et al., 2010] and to the correlation coefficient between MOD16 estimates and observations (Table 3). Our methodology demonstrated that the P-M equation could be derived by remotely sensed data for ET estimates at 8-days and annual "timescales and has the potential for regional and global applications".

The RS-PMPT model underestimation of the peak tower ET for some of the sites can be related to errors in the estimated VPD. Analysis of the VPD model for all the 20 sites showed that it tended to overestimate the tower VPD with a MAE of 0.46 kPa with the highest overestimation detected for sites with temperature higher than 40ºC (data not shown). High VPD will result in an increase in the modeled surface resistance and thus the RS-PMPT model will underestimate the observed ET estimates. The differences in the RS-PMPT ET estimates across sites were related to variability in soil moisture, environmental constraint, and LAI. For the deciduous calibration sites with similar LAI, RS-PMPT model performed better for the US-Ha1 site than the more humid US-MMS site mostly due to underestimating canopy transpiration because of possible overestimation of canopy surface wetness (f_{wet}) at the US-MMS site. It is expected that the model will exhibit strong temperature constraints for sites with temperature reaching more than 35^{0}C due to the parameters of the $f(T_S)$ function.

The RS-PMPT modeled ET was able to capture successfully the seasonality of the observed ET for the semiarid sites (US-Seg and US-Wkg sites) dominated by short grasses, but failed for the shurbland site (Sky Oaks). In the chaparral vegetation at Sky Oaks, LAI changes drastically in relation to water availability [Sims et al., 2006] and might be adapted to higher T_{opt} than the T_{opt} used in our model. Consequently, a generalized T_{opt} would not be expected to apply to all sites and conditions especially for the drought sites as T_{opt} could be driven by drought effects than temperature [Sims et al., 2008].

"Analyzing the results for the Vaira Ranch site, we noticed that RS-PMPT was mostly dominated by soil evaporation during the overestimation period (Fig. 4). f_{SM} is assumed to represent both canopy and soil water content if T_s includes both vegetation and soil components, which is the case for MODIS LST [Vertraeten et al., 2006]. It can be assumed that f_{SM} might have overestimated soil moisture content, causing the RS-PMPT model to overestimate tower ET at the end of the growing season for Vaira Ranch site (Fig. 4). Whereas, for the US-IB2 grassland site, f_{SM} is limiting soil evaporation due to errors in the ATI retrieval from satellite land surface temperature causing the model to underestimate flux tower ET. In addition, MODIS pixel for the US-IB2 site included parcels of adjacent crop and grasslands [Wagle et al., 2017] that would impact the MODIS data and the modeled ET estimates for this site. The influence of the adjacent crop that has on observed ET for the US-IB2 site is beyond the scope of this study, but it possibly explains the high observed ET values for this site."

The RS-PMPT model "improved the ET estimates at most of the study sites" compared to MOD16 (Table 3). Furthermore, the RS-PMPT produced accurate 8-day ET "estimates by reducing MAE and RMSE for 14 of the 20 flux tower sites and" with average r^2 of 0.84 and MAE of 0.33 W/m^2. More importantly, the RS-PMPT bias for all the study sites was on average 36% lower than the MOD16 (MSE_S/MSE, Table 3). Considering that our ET results showed low biases (lower MAE and RMSE), higher d, and high r^2 for the validation sites, the RS-PMPT model was able to capture successfully the observed seasonal and interannual variability and the site to site differences in ET. The biases that existed between RS-PMPT model and the flux tower ET observations probably were influenced by:

1) Missing flux data and energy balance closure: The tower flux latent heat data is usually available for every hour or half an hour interval. Some of the daily observations for the flux towers used were missing due to system errors. In addition, many days were missing several hourly or half an hour observations. The use of fewer flux observations to estimate daily averages of ET can lead to errors in the model error analysis [Desai et al., 2005; Dragoni et al., 2007; Hollinger and Richardson, 2005]. In addition, energy closure issue in the flux measurements is an important factor that can cause the difference between the model estimates and flux estimates and can introduce discrepancy with the observed ET [Franssen et al., 2010; Leuning et al., 2012; Stokli et al., 2008]. For instance, Wilson et al., [2002] showed that for 22 flux observed sensible and latent heat underestimated available energy by 20%. Thus, systematic

underestimation by the Eddy covariance measurements due to for example, vegetation heat storage and missing advection of heat and water vapor, could explain the overestimation in the RS-PMPT estimates for some of the sites.

2) Scaling from flux to MODIS: The flux tower footprint is about 1 km^2 around the tower and its direction is influenced by local environmental conditions such as wind speed and direction [Schmid, 2002]. Comparison of the flux observed ET with RS-PMPT estimates estimated from the 3 × 3 1-km^2 averaged MODIS data could have introduced uncertainties due to the difference in the pixel size, flux footprint, and the varying environmental conditions in each site.

3) Algorithm limitations: The following limitations in our model perhaps contributed to the difference between the model estimate and the flux observations: (1) Our simplified model was developed using generalized relationships to estimate surface conductance and aerodynamic resistance using universal parameters instead of biome specific parameters. However, these parameters do differ for different biome types; (2) Empirical relationships were used to estimate certain variables and parameters that can introduce biases to our model. For instance, VPD was able to explain 85% of the variability in the corresponding tower measurements with a MAE of 0.35 kPa (data no shown). The unexplained variability could have introduced errors to our estimates. As mentioned previously, overestimating tower VPD can lead to underestimation of measured ET; (3) Uncertainties in the mechanism controlling soil heat flux. As a result, we might have overestimated soil heat flux for the dry sites and underestimated ET. In addition, the RS-PMPT might not include all the parameters that could

influence ET (e.g. topography and its effect on available soil moisture) and incorporating rooting zone soil moisture need to be explored in the future.

"Finally, in implementing our approach, several assumptions were made to achieve simplicity and applicability of RS-PMPT model. For instance, the physiological variables such as r_a and r_c were estimated using minimum number of parameters, resulting in minimizing the number of model parameters needed to run the RS-PMPT model. The tradeoff between the use of our canopy resistance model compared to previous studies might have a minimal effect on our results without influencing the overall model accuracy (Fig. 2-10). In addition, parameters of the the r_a and r_s models have been estimated in this study without relying on flux tower-based data such as wind speed and humidity. Moreover, our canopy resistance values ranged from 100 to 1000 sm^{-1} similar to the values reported in the literature for deciduous forests [Li et al., 2009]."

5 Conclusion

Evapotranspiration is one of the most important parameters of the water cycle and accurate estimation of ET dynamic is essential for better understanding of the changes in the hydrological cycle. Here, we presented a different operational approach to derive the P-M equation solely by remotely sensing data. The RS-PMPT model was developed and validated at 20 flux tower sites representative of North America major ecosystem types. The results revealed that the RS-PMPT model matched the magnitude and seasonal variation of the measured ET. In addition, the RS-PMPT model performance was very similar and in some cases even better than the MOD16. The daily MAE and RMSE was reduced from 0.54 mm/day and 0.68 mm/day from the MOD16 to 0.33 mm/day and 0.46 mm/day with our RS-PMPT mode, respectively. The significant relationship between RS-PMPT estimates and the tower ET observations implied that the RS-PMPT model has the potential to be applied to different ecosystems and can be implemented at different spatial scales.

Because of the application of the RS-PMPT model, we have demonstrated that our approach can operate without the need for site-based meteorological or climate reanalysis data and permits the RS-PMPT model application to areas lacking surface measurements. Secondly, the algorithm can incorporate data from several satellite sensors. Sources of errors in the model can be improved by reducing the errors in the estimated VPD and by including root zone soil moisture. The RS-PMPT precision is dependent in satellite data and any improvements in remote sensing data accuracy will enhance the RS-PMPT ET estimates.

We have learned from this experiment that capturing the peak of the observed ET in a yearly basis is a challenge to the modeling community. Local site conditions such as, soil type and species composition, might play an important role in determining the peak observed ET. Our next step is to include leaf wetness to improve the canopy resistance model and to experiment with the use of canopy cover fraction from the soon to be lunched Global Ecosystem Dynamics Investigation (GEDI) to enhance model energy partitioning between the vegetation and the soil.

Acknowledgment

We acknowledge the following AmeriFlux sites for their data records: US-Har1, US-MMS, US-UMB, US-Ho1, US-SP1, US-DK3, US-FPe, US-IB2, US-Kon, US-MOz, US-Seg, US-SO3, US-Ton, US-Var, US-WBW, US-Wkg. US-Bkg, CA-Oas, CA-Let, CA-Man. We would like to thanks AmeriFlux for the tower data and ORNL for the MODIS data. Funding for AmeriFlux data resources was provided by the U.S. Department of Energy's Office of Science. We would like to thank the reviewers for al their feedbacks and effort to improve this manuscript.

Reference:

Allen, R.G., M.E. Jensen, J.L. Wright, R.D. Burman (1989). Operational estimates of reference evapotranspiration. Agronomy Journal, 81(4), 650-662.

Anderson-Teixeira, K.J., J.P. Delong, A.M. Fox, D.A. Brese, M.E. Litvak (2011). Differential responses of production and respiration to temperature and moisture drive the carbon balance across a climatic gradient in New Mexico. Global Change Biology, 17, 410424.

Baldocchi, D., E. Falge, L. Gu, R. Olson, D. Hollinger, S. Running, P. Anthoni, C. Bernhofer, K. Davis, R. Evans, J. Fuentes, A. Goldstein, G. Katul, B. Law, X. Lee, Y. Malhi, T. Meyers, W. Munger, W. Oechel, K. T. Paw, U.K. Pilegaard, H.P. Schmid, R. Valentini, S. Verma, T. Vesala, K. Wilson, and S. Wofsy (2001). FLUXNET: A new tool to study the temporal and spatial variability of ecosystem-scale carbon dioxide, water vapor, and energy flux densities. Bulletin of the American Meteorological Society, 82, 2415-2434.

Barr, A.G., T.A. Black, E.H. Hogg, T.J. Griffis, K. Morgenstern, N. Kljun, A. Theede, Z. Nesic (2007). Climatic control on the carbon and water balances of a boreal aspen forest, 1994-2003. Global Change Biology, 13, 561-576.

Bastiaanssen W. G. M., M. Menenti, R. A. Feddes, A. A. M. Holtslag (1998a). A remote sensing surface energy balance algorithm for land (SEBAL). 1. Formulation. Journal of Hydrology, 212-213, 198-212.

Bastiaanssen, W. G. M., H. Pelgrum, J. Wang, Y. Ma, J. F. Moreno, G. J. Roerink, T. van der Wal (1998b). A remote sensing surface energy balance algorithm for land (SEBAL). 2: Validation. Journal of Hydrology, 212-213, 213-229.

Beer, C., M. Reichstein, P. Ciais, G.D. Farquhar, D. Papale (2007). Mean annual GPP of Europe derived from its water balance. Geophysical Research Letters, 34, L05401, doi:10.1029/2006GL029006,

Beer, C, P. Ciais, M. Reichstein, D. Baldocchi, B.E. Law, D. Papale, J-F. Soussana, C. Ammann, N. Buchmann, D. Frank, D. Gianelle, I.A. Janssens, A. Knohl, B. Köstner, E. Moors, O. Roupsard, H. Verbeeck, T. Vesala, C.A. Williams, G. Wohlfahrt (2009). Temporal and among-site variability of inherent water use efficiency at the ecosystem level. Global Biogeochemical Cycles, 23, GB2018, doi:10.1029/2008GB003233

Chaves, M.M. (1991). Effects of water deficits on carbon assimilation. Journal of Experimental Botany, 42 (234), 116.

Cleugh, H. A., R. Leuning, Q. Mu, S.W. Running (2007). Regional evaporation estimates from flux tower and MODIS satellite data. Remote Sensing of Envrionment, 106 (3), 285-304.

Damour, G., T. Simmoneau, H. Cochard, L. Urban (2010). An overview of stomatal conductance at leaf level. Plant, Cell, and Environment, 33, 1419-1438.

Desai, A.R., P.V. Bolstad, B. D. Cook, K. J. Davis, E.V. Carey (2005). Comparing net ecosystem exchange of carbon dioxide between an old-growth and mature forest in the upper Midwest, USA. Agricultural and Forest Meteorology, 128 (1), 33-55.

Dingman, S. L. 2002. *Physical Hydrology*. 2nd ed. Prentice Hall.

Doelling, D.R., N.G. Loeb, D.F. Keyes, M.L. Nordeen, D. Morstad, C. Nguyen, B.A. Wielicki, D.F. Young, M. Sun. (2013). Geostationary enhanced temporal interpolation for CERES flux products. Journal of Atmosphere and Oceanic Technology, 30, 1072-1090.

Dorigo, W.A., Wagner, W., Albergel, C., Albrecht, F., Balsamo, G., Brocca, L., Chung, D., Ertl, M., Forkel, M., Gruber, A., Haas, E., Hamer, D. P. Hirschi, M., Ikonen, J., De Jeu, R. Kidd, R. Lahoz, W., Liu, Y.Y., Miralles, D., Lecomte, P. (2017). ESA CCI Soil Moisture for improved Earth system understanding: State-of-the art and future directions. Remote Sensing of Environment, 2017, ISSN 0034-4257, https://doi.org/10.1016/j.rse.2017.07.001.

Dragoni, D, H.P. Schmid, C.S.B. Grimmond, H.W. Loescher (2007). Uncertainty of annual net ecosystem productivity estimated using eddy covariance flux measurements. Journal of Geophysical Research D: Atmos.112, D17102, doi:10.1029/2006JD008149.

Ershadi A., M.F McCabe, J.P. Evans, N.W. Chaney, E.F. Wood (2014). Multi-site evaluation of terrestrial evaporation models using FLUXNET data. Agricultural and Forest Meteorology, 187, 46-61.

Farquhar, G.D., T.D. Sharkey (1982). Stomatal conductance and photosynthesis. Annual Review of Plant Physiology, 33, 317-345.

Fisher, J.B., K.P. Tu, D.D. Baldocchi (2008). Global estimates of the land–atmosphere water flux based on monthly AVHRR and ISLSCP-II data, validated at 16 FLUXNET sites. Remote Sensing of Environment, 112, 901–919.

Fisher, J.B., F. Melton, E. Middleton, C. Hain4, M. Anderson, R. Allen, M.F. McCab , S. Hook, D. Baldocch9 , P.A. Townsend, A. Kilic, K. Tu , D.D. Miralles , J. Perret, J-P. Lagouarde, D. Waliser , A.J. Purdy , A. French , D. Schimel, J.S. Famiglietti, G. Stephen, E.F. Wood (2017). The future of evapotranspiration: Global requirements for ecosystem functioning, carbon and climate feedbacks, agricultural management, and water resources. Water Resources Research, 53, 2618–2626, doi:10.1002/2016WR020175.

Flanagan, L.B., A.C. Adkinson (2011). Interacting controls on productivity in a northern Great Plans grassland and implications for response to ENSO events. Global Change Biology, 17, 3293-3311.

Franssen, H.J. H, R. Stöckli, I. Lehner,, E. Rotenberg,, S.I. Seneviratne (2010). Energy balance closure of eddy-covariance data: A multisite analysis for European FLUXNET stations. . Agricultural and Forest Meteorology, 150, 1553-1567.

García, M., I. Sandholt, P. Ceccato, M. Ridler, E. Mougin, L., Kergoat, L. Morillas, F. Timouk, R. Frensholt, F. Domingo (2013). Actual evapotranspiration in drylands derived from in-site and satellite data: Assessing biophysical constraints. Remote Sensing of Environment, 131, 103-118.

Gerosa, G., S. Mereu, A. Finco, R. Marzuoli (2012). Stomatal conductance modeling to estimate evapotranspiration of natural and agricultural ecosystems. Evapotranspiration -Remote Sensing and Modeling, Dr. Ayse Irmak (Ed.), ISBN: 978-953-307-808-3.

Goulden, M.L. (1996). Carbon assimilation and water-use efficiency by neighboring Mediterranean-climate oaks that differ in water access. Tree Physiology, 16, 417-424.

Granger, R.J. (2002). Satellite-derived estimates of evapotranspiration in the Gediz basin. Journal of Hydrology, 229, 70-76.

Grimmond, C.S.B., P.J. Hanson, F. Cropley, H.P. Schmid, S. Wullschleger (2000). Evapotranspiration rates at the Morgan Monroe State Forest Ameriflux site: a comparison of results from eddy covariance turbulent flux measurements and sap flow techniques. In: 15th Conference on Hydrology, American Meteorological Society, Long Beach, CA, pp. 158–161.

Gu. L., T. Meyers, S.G. Oallardy, P.J. Hanson, B. Yang, M. Heuer, K.P. Hosman, Q. Liu, J.S. Rigges, D. Sluss, S.D. Wullschleger (2007). Influences of biomass heat and biochemical energy storages on the land surface fluxes and radiative temperature. Journal of Geophysical Research, 112, D02107, doi:10.1029/2006JD007425.

Hashimoto, H., J.L. Dungan, M.A. White, F. Yang, A.R. Michaelis, S.W. Running, R.R. Nemani (2008). Satellite-based estimation of surface vapor pressure deficits using MODIS land surface temperature data. Remote Sensing of Environment, 112 (1), 142-155.

Hollinger, D.Y, A.D. Richardson (2005). Uncertainty in eddy covariance measurements and its application to physiological models. Tree Physiology, 25, 873-885.

Hunt, E.R., S.C. Piper, R. Nemani, C.D. Keeling, R.D. Otto, S.W. Running (1996). Global net carbon exchange and intra-annual atmospheric CO2 concentrations predicted by an ecosystem processes model and three-dimensional atmospheric transport model. Global Biogeochemical Cycles, 10 (3), 431-456

Jarvis, P.G. (1976). The interpretation of the variation in leaf water potential and stomatal conductance found in canopies in the field. Philosophical Transactions of the Royal Society of London, 273, 593-610.

Jiang, L., S. Islam (2001). Estimation of surface evaporation map over Southern Great Plains using remote sensing data. Water Resources Research, 37 (2), 329-340.

Jiang, L., S. Islam, W. Guo, A.S. Jutla, S. U.S. Senarath, B.H. Ramsay, E. Eltahir (2009). A satellite-based Daily Actual Evapotranspiration estimation algorithm over South Florida. Global and Planetery Change, 67 (1), 62-77.

Katul, G., C-I. Hsieh, D. Bowling, K. Clark, N. Shurpali, A. Turnispeed, J. Albertson, K. Tu, D. Hollinger, B. Evans, B. Offerle, D. Anderson, D. Ellsworth, C. Vogel, R. Oren (1999). Spatial variability of turbulent fluxes in the roughness sublayer of an even-aged pine forest. Boundary-Layer Meteorology, 93, 1-28.

Kustas, W.P., J.M. Norman (1999). Evaluation of soil and vegetation heat flux predictions using a simple two-source model with radiometric temperatures for partial canopy cover. Agricultural and Forest Meteorology, 94 (1), 13-29.

Law, B.E., E. Falge, L. Gu, D.D. Baldocchi, P. Bakwin, P. Berbigier, K. Davis, A.J. Dolman, M. Falk, J.D. Fuentes, A. Goldstein, A. Granier, A. Grelle, D. Hollinger, I.A. Janssens, P. Jarvis, N.O. Jensen, G. Katul, Y. Mahli, G. Matteucci, T. Meyers, R. Monson, W. Munger, W. Oechel, R. Olson, K. Pilegaard, K.T. Paw U, H. Thorgeirsson, R. Valentini, S. Verma, T. Vesala, K. Wilson, S. Wofsy (2002). Environmental controls over carbon dioxide and water vapor exchange of terrestrial vegetation. Agricultural and Forest Meteorology, 113, 97-120.

Leuning, R., Y. Q. Zhang, A. Rajaud, H. Cleugh, K. Tu (2008). A simple surface conductance model to estimate regional evaporation using MODIS leaf area index and the Penman-Monteith equation. Water Resources Research. 44, doi:10.1029/2007WR006562.

Leuning, R., E, van Gorsel, W.J. Massman, P.R. Isaac (2012). Reflections on the surface energy imbalance problem. Agricultural and Forest Meteorology, 156, 65-74.

Li, R., Q. Min, and B. Lin (2009). Estimation of evapotranspiration in a mid-latitude forest using the Microwave Emissivity Difference Vegetation Index (EDVI). Remote Sensing of Environment, 113, 2011-2018.

Long, D., V.P. Singh (2010). Integration of the GG model with SEBAL to produce time series of evapotranspiration of high spatial resolution at watershed scales, Journal of Geophysical Research, 115, D21128, doi:10.1029/2010JD014092.

Long, D, V.P. Singh (2012). A two-source trapezoid model for evapotranspiration (TME) from satellite imagery. Remote Sensing of Vegetation, 121, 370-388

Maidment, D.R. (1993). Handbook of hydrology: McGraw-Hill. ISBN: 0070397325/9780070 397323.

Matamal, R., J.D Jastrow, R.M. Miller, C.T. Garten (2008). Temporal changes in C and N stocks of restored prairie: Implications for C sequestration strategies. Ecological Application, 18960, 1470-1488.

Mattas, C., B. Franch, J.A. Sobrino, C. Corbari , J.C. Jiménez-Muñoz, L. Olivera-Guerra, D. Skokovic, G. Sória, R. Oltra-Carriò, Y. Julien, M.Mancini (2014). Impacts of the broadband albedo on actual evapotranspiration estimated by S-SEBI model over an agricultural area. Remote Sensing of Environment, 147, 23-42.

McCabe, M.F., A. Ershadi, C. Jimenez, D.G. Miralles, D. Michel, E.F. Wood (2016). The GEWEX LandFlux project: evaluation of model evaporation using tower-based and globally gridded forcing data. Geoscientific Model Development, 9, 293-305.

Michel, D, C. Jiménez, D.G. Miralles, M. Jung, M. Hirschi, A. Ershadi, B. Mertens, M.F. McCabe, J.B. Fisher, Q. Mu, S.I. Seneviratne, E.F. Wood, D. Fernández-Prieto (2016). The WACMOS-ET project-Part 1: Tower-scale evaluation of four remote-sensing-based evapotranspiration algorithms. Hydrology and Earth System Science, 20, 803-822.

McVicar, T.R., D.L.B. Jupp (1999). Estimating one-time-of-day meteorological data from standard daily data as inputs to thermal remote sensing based energy balance models. Agricultural and Forest Meteorology, 96 (4), 219-238.

McVicar, T.R., D.L.B Jupp (2002). Using covariates to spatially interpolate moisture availability in the Murray-Darling Basin: A novel use of remotely sensed data. Remote Sensing of Envrionment, 79 (2), 199-212.

Medrano, H., J.M. Escalona, J. Bota, J. GulÍas, J. Flexas (2002). Regulation of photosynthesis of C_3 plants in response to progressive drought: Stomatal conductance as a reference parameter. Annual Botany, 89, 895-905.

Merlin, O., J. Chirouze, A. Olioso, L. Jarlan, G. Chehbouni, G. Boulet (2014). An image-based four source surface energy balance model to estimate crop evapotranspiration from solar reflectance/thermal emission data (SEB-4S). Agricultural and Forest Meteorology, 184, 188-203

Monteith, J.L. (1965). Evaporation and environment. Symposia of the Society for Experimental Biology, 19, 205-234.

Mildrexler, D.J., M. Zhao, S.W. Running (2011). A global comparison between station air temperatures and MODIS land surface temperatures reveals the cooling role of forests. Journal of Geophysical Research, 116, G03025, doi:10.1029/2010JG001486.

Miralles, D.G., C. Jimenez, M. Jung, D. Michel, A. Ershadi, M.F. McCabe, M. Hirschi, B. Martens, A.J. Dolman, J.B. Fisher, Q. Mu, S.I. Seneviratne, E.F. Wood, D. Fernámdez-Prieto (2016). The WACMOS-ET project-Part 2: Evaluation of global terrestrial evaporation data sets. Hydrology and Earth System Sciences, 20, 823-842.

Mu, Q., F.A. Heinsch, M. Zhao, S.W. Running (2007). Development of a global evapotranspiration algorithm based on MODIS and global meteorology data. Remote Sensing of Envrionment, 111 (4), 519-536.

Mu, Q., M. Zhao, S.W. Running (2011). Improvements to a MODIS global terrestrial evapotranspiration algorithm. Remote Sens. Environ., 115, 1781-1800.

Myneni, R., Knyazikhin, Y., Park, T. (2015). MOD15A2H MODIS/Terra Leaf Area Index/FPAR 8-Day L4 Global 500m SIN Grid V006. NASA EOSDIS Land Processes DAAC. https://doi.org/10.5067/MODIS/MOD15A2H.006.

Nemani, R.R., S.W. Running (1989). Estimation of Regional Surface Resistance to Evapotranspiration from NDVI and Thermal-IR AVHRR Data. Journal of Applied Meteorology, 28 (4), 276-284.

Nishida, K., R.R. Nemani, S.W. Running, J.M. Glassy (2003). An operational remote sensing algorithm of land surface evaporation. Journal of Geophysical Research D: Atom., 108 (4270),doi:10.1029/2002JD002062.

Norman, J.M., W.P. Kustas, K.S. Humes (1995). Source approach for estimating soil and vegetation energy fluxes in observations of directional radiometric surface temperature. Agricultural and Forest Meteorology, 77 (3), 263-293.

ORNL DAAC. 2008. MODIS Collection 5 Land Product Subsets Web Service. ORNL DAAC, Oak Ridge, Tennessee, USA. https://doi.org/10.3334/ORNLDAAC/1252.

Powell, T.L., H.L. Gholz, K.L. Clark, G. Starr, W.P., Cropper, T.A. Martin (2008). Carbon exchange of a mature, naturally regenerated pine forest in north Florida. Global Change Biology, 14, 2523-2538.

Priestley, C.H. B., R.J. Taylor (1972). On the assessment of surface heat flux and evaporation using large-scale parameters. Monthly Weather Review, 100, 81–92.

Running, S.W., J.C. Coughlan (1988). A general model of forest ecosystem processes for regional applications I. Hydrologic balance, canopy gas exchange and primary production processes. Ecological Modeling, 42 (2), 125-154.

Running, S., Mu, Q., Zhao, M. (2017). MOD16A2 MODIS/Terra Net Evapotranspiration 8-Day L4 Global 500m SIN Grid V006. NASA EOSDIS Land Processes DAAC. https://doi.org/10.5067/MODIS/MOD16A2.006.

Schaaf, C., Wang, Z. (2015). MCD43A1 MODIS/Terra+Aqua BRDF/Albedo Model Parameters Daily L3 Global - 500m V006. NASA EOSDIS Land Processes DAAC. https://doi.org/10.5067/MODIS/MCD43A1.006.

Schmid, H.P. (2002). Footprint modeling for vegetation atmosphere exchange studies: A review and prospective. Agricultural and Forest Meteorology, 113, 159-183.

Schmid, H.P., H.B. Su, C.S. Vogel, P.S. Curtis (2003). Ecosystem-atmosphere exchange of carbon dioxide over a mixed hardwood forest in northern lower Michigan. Journal of Geophysical Research, 108, D14, 4417. doi:10.1029/2002JD003011

Schulze. E.D., F.M. Kelliher, C. Korner, J. Lloyd, R. Leuning (1994). Relationships among maximum stomatal conductance, ecosystem surface conductance, carbon assimilation rate, and plant nitrogen nutrition: A global ecology scaling exercise. Annual Review of Eco logical Systems, 25, 629-660.

Scott, R.L. (2010). Using watershed water balance to evaluate the accuracy of eddy covariance evaporation measurements for three semiarid ecosystems. Agricultural and Forest Meteorology, 150, 219-225.

Sims, D.A., H. Luo, S. Hastings, W.C. Oechel, A.F. Rahman, J.A. Gamon (2006). Parallel adjustments in vegetation greenness and ecosystem CO2 exchange in response to drought in a Southern California chaparral ecosystem. Remote Sensing of Environment, 103, 289–303.

Sims, D.A., A.F Rahman, V.D. Cordova, B.Z. El-Masri, D.D. Baldocchi, P.V. Bolstad, L.B. Flanagan, A.H. Goldstein, D.Y. Hollinger, L. Misson, R.K., Monson, W.C. Oechel, H.P. Schmid, S.C. Wofsy, L. Xu (2008). A new model of gross primary production for North American ecosystems based solely on the enhanced vegetation index and land surface temperature from MODIS. Remote Sensing of Environment, 112, 1633-1646.

Smith, G., Priestley, K., Loeb, N., Wielicki, B., Charlock, T., Minnis, P., Doelling, D., Rutan, D. (2011). Clouds and Earth Radiant Energy System (CERES), a review: Past, present and future. Advances in Space Research, 48, 254–263.

Stewart, J.B. (1977). Evaporation from the wet canopy of a pine forest. Water Resources Research, 6(3), 915-912.

Stewart, J.B. (1988). Modeling surface conductance of pine forest. Agricultural and Forest Meteorology, 43, 19-35.

Stewart, J.B., L.W. Gary (1989). Preliminary modeling of transpiration from the FIFE site in Kansas. Agricultural and Forest Meteorology, 48, 305-315.

Su, Z. (2002). The Surface Energy Balance System (SEBS) for estimation of turbulent heat fluxes. Hydrology and Earth System Sciences, 6 (1), 85-99.

Thornton, P.E. (1998). Regional ecosystem simulation: combining surface- and satellite-based observations to study linkages between terrestrial energy and mass budgets. Ph.D. dissertation. School of Forestry, University of Montana, Missoula MT, 280 pp.

Van der Tol, C., J.H.C. Gash, S.J. Grant, D.D. McNeil, M. Robinson (2003). Average wet canopy evaporation for a Sitka spruce forest derived using the eddy correlation-energy balance technique. Journal of Hydrology, 273, 12-19.

Vinukollu, P.K., E.R. Wood, C.R. Ferguson, J.B. Fisher (2011). Global estimates of evapotranspiration for climate studies using multi-sensor remote sensing data: Evaluation of three process-based approaches. Remote Sensing of Environment, 115, 801-823.

Wagle, P., X. Xiao, P. Gowda, J. Basara, N. Brunsell, J. Steiner, A. K.C (2017). Analysis and estimation of tallgrass prairie evapotranspiration in the central United States. Agricultural and Forest Meteorology, 232, 35-47.

Wan, Z., Hook, S., Hulley, G. (2015). MOD11A2 MODIS/Terra Land Surface Temperature/Emissivity 8-Day L3 Global 1km SIN Grid V006. NASA EOSDIS Land Processes DAAC. https://doi.org/10.5067/MODIS/MOD11A2.006

Wielicki, B.A., Barkstrom, B.R., Harrison, E.F., Lee, R.B., Louis Smith, G., Cooper, J.E. (1996). Clouds and the Earth's Radiant Energy System (CERES): An earth observing system experiment. Bulletin of the American Meteorological Society, 77, 853–868.

Willmott, C. J. (1981). On the validation of models. Physical Geography, 2 (2), 184−194.

Willmott, C. J. (1982). Some comments on the evaluation of model performance. Bulletin of the American Meteorological Society, 63 (11), 1309−1313.

Willmott C.J, S.M. Robeson, and K. Matsuura, (2011). A refined index of model performance. International Journal of Climatology, doi: 10.1002/joc.2419.

Wilson, G.W.T., D.C. Hartnett, M.D. Smith, K. Kobbeman (2001). Effects of Mycorrhizae on growth and demography of tallgrass prairie forbs. American Journal of Botany, 88(80, 1452-1457.

Wilson K., A. Goldstein, E. Falge, M. Aubinet, D. Baldocchi, P. Berbigier, C. Bernhofer, R. Ceulemans, H. Dolman, C. Field, A. Grelle, A. Ibrom, B.E. Law, A. Kowalski, T. Meyers, J. Moncrieff, R. Monson, W. Oechel, J. Tenhunen, R. Valentini, S. Verma (2002). Energy balance closure at FLUXNET sites. Agricultural and Forest Meteorology, 113, 223-243.

Wong, S.C., I.R. Cowan, G.D. Farquhar (1979). Stomatal conductance correlates with photosynthetic capacity. Nature (London), 282**,** 424-6.

Xu, L., Baldocchi, D.D. (2004). Seasonal variation in carbon dioxide exchange over a Mediterranean annual grassland in California. Agricultural and Forest Meteorology, 123, 79-96

Yang, W., D. Huang, B. Tan, J.C. Stroeve, N.V. Shabanov, Y. Knyazikhin, R.R. Nemani, R.B. Myneni (2006). Analysis of leaf area index and fraction of PAR absorbed by vegetation products from the Terra MODIS Sensor: 2000–2005. IEEE Transaction on Geosciences and Remote Sensing, 44(7), 1829-1872

Yang, Y., S. Shang (2013). A hybrid dual-source scheme and trapezoid framework-based evapotranspiration model (HTEM) using satellite images: Algorithm and model test. Journal of Geophysical Research: Atmosphere, 118, 2284-2300.

Yang, Y., D. Long, H. Guan, W. Liang, C. Simmons, O. Batelaan (2015). Comparison of three dual-source remote sensing evapotranspiration models during the MUSOEXE-12 campaign: Revisit of model physics. Water Resources Research, 51, 3145–3165, doi:10.1002/2014WR015619.

Yang, Y.Z., W.H. Cai, J. Yang (2017). Evaluation of MODIS land surface temperature data to estimate near-surface air temperature in Northeast China. Remote Sensing, 9, 410, doi:10.3390/rs9050410.

Yao, Y., S. Liang, J. Cheng, S. Liu, J.B., Fisher, Z. Zhang, K. Jia, X. Zhao, Q. Qin, B. Zhao, A. Han, G. Zhao, G. Zhao, Y. Li, S. Zhao (2013). MODIS-driven estimation of terrestrial latent heat flux in China based on a modified Priestley-Taylor algorithm. Agricultural and Forest Meteorology, 171-172, 187-202.

Yao, Y., S. Liang, X. Li, J. Chen, S. Liu, K. Jia, X. Zhang, Z. Xiao, J.B. Fisher, Q. Mu, M. Pan, M. Liu, J. Cheng, B. Jiang, X. Xie, T. Grünwald, C. Bernhofer, O. Roupsard (2017). Improving global terrestrial evapotranspiration estimation using support vector machine by integrating three process-based algorithms. Agricultural and Forest Meteorology, 242, 55-74.

Zhang, Y.Q., F.H.S. Chiew, L. Zhang, R. Leuning, H.A. Cleugh (2008). Estimating catchment evaporation and runoff using MODIS leaf area index and the Penman-Monteith equation. Water Resources Research, 44, doi:10.1029/2007WR006563.

Zhang, K., J.S. Kimball, R.R. Nemani, S.W. Running (2010). A continuous Satellite-derived global record of land surface evapotranspiration from 1983-2006. Water Resources Research, 46, W09522, doi:10.1029/2009WR008800.

Zhang, K., J.S. Kimball, S.W. Running (2016). A review of remote sensing based actual evapotranspiration estimation. Water, 3, 834-853.

Figure Captions

Figure 1. Flowchart of the RS_ET model. LAI: Leaf Area Index; T_S: MODIS LST; fpar: Fraction of photosynthetic active radiation; T_a: Air temperature; e_s= saturated vapor pressure; VPD: Vapor pressure deficit; R_l: net long wave radiation; R_s: net shortwave radiation; R_n: net radiation; G: Ground heat flux; R_{soil} : Net radiation to the soil.

Figure 2. Seasonal time series of daily ET for the calibration deciduous sites either at eddy flux tower (open circle) or predicted by the RS-PMPT model (black line), or MODIS ET (dashed lines).

Figure 3. Seasonal time series of daily ET for the calibration evergreen forest sites either at eddy flux tower (open circle) or predicted by the RS-PMPT model (black line), or MODIS ET (dashed lines).

Figure 4. Seasonal time series of daily ET for the calibration grassland sites either at eddy flux tower (open circle) or predicted by the RS-PMPT model (black line), or MODIS ET (dashed lines).

Figure 5. Seasonal time series of daily ET for the shrubland and savanna site either at eddy flux tower (open circle) or predicted by the RS-PMPT model (black line), or MODIS ET (dashed lines).

Figure 6. Average 8-day of the RS-PMPT ET estimates compared with average 8-day eddy flux tower ET for the calibration sites. The dashed line is the regression line and the black solid line is the 1:1 line. The dashed line is the regression line and the black solid line is the 1:1 line. The data for each site represent the average 8-day data for the years included in the study (see Table 2)

Figure 7. Seasonal time series of daily ET for the validation deciduous sites either at eddy flux tower (open circle) or predicted by the RS-PMPT model (black line), or MODIS ET (dashed lines).

Figure 8. Seasonal time series of daily ET for the validation evergreen forest sites either at eddy flux tower (open circle) or predicted by the RS-PMPT model (black line), or MODIS ET (dashed lines).

Figure 9. Seasonal time series of daily ET for the validation grassland sites either at eddy flux tower (open circle) or predicted by the RS-PMPT model (black line), or MODIS ET (dashed lines).

Figure 10. Average 8-day of the RS-PMPT ET estimates compared with average 8-day eddy flux tower ET for the validation sites. The dashed line is the regression line and the black solid line is the 1:1 line. The data for each site represent the average 8-day data for the years included in the study (see Table 2)

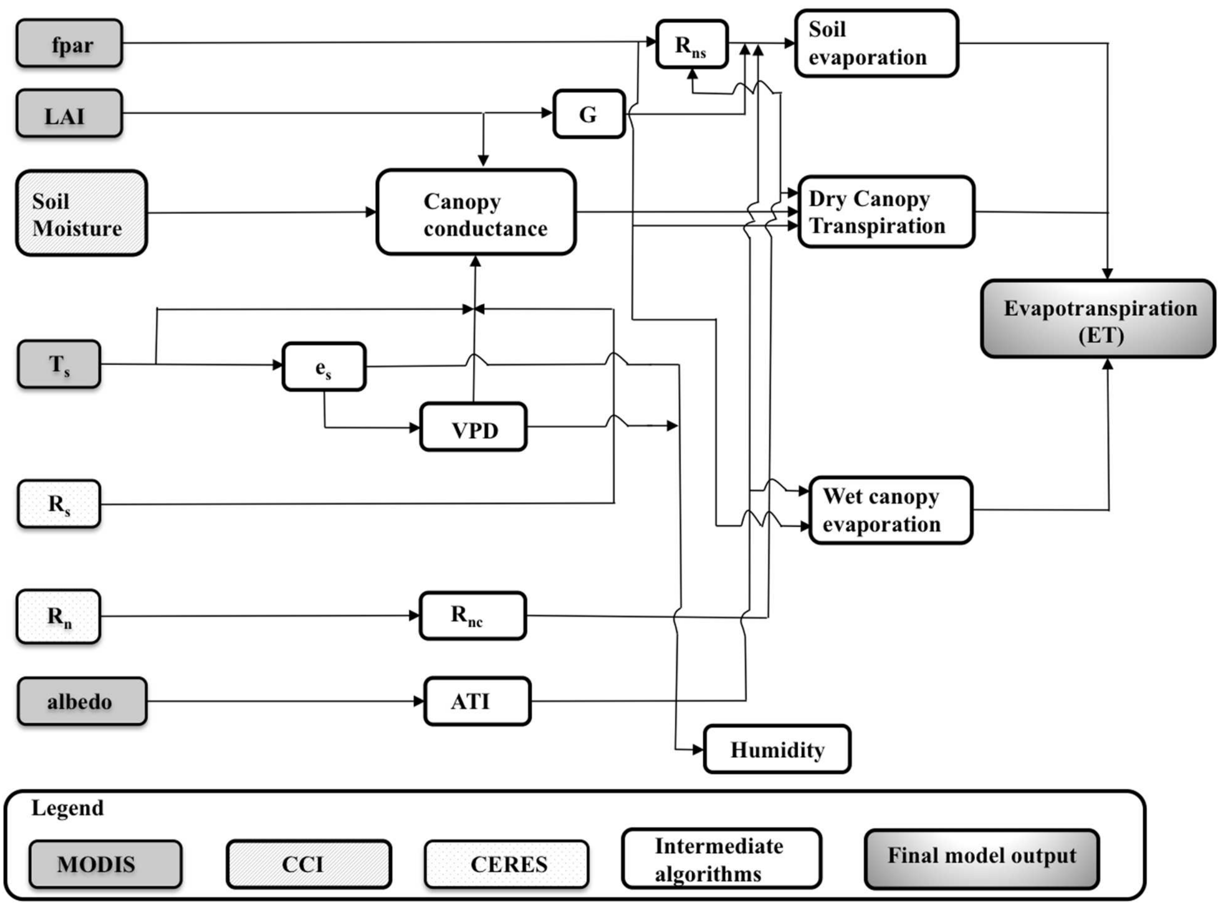

Figure 1. Flowchart of the RS_ET model. LAI: Leaf Area Index; T_S: MODIS LST; fpar: Fraction of photosynthetic active radiation; T_a: Air temperature; e_s= saturated vapor pressure; VPD: Vapor pressure deficit; R_s: net shortwave radiation; R_n: net radiation; G: Ground heat flux; R_{ns} : Net radiation to the soil.

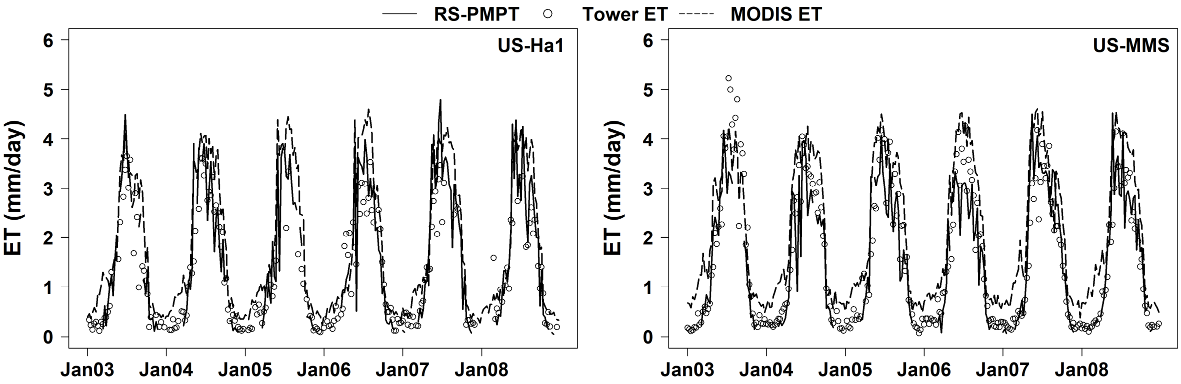

Figure 2. Seasonal time series of daily ET for the calibration deciduous sites either at eddy flux tower (open circle) or predicted by the RS-ET model (black line).

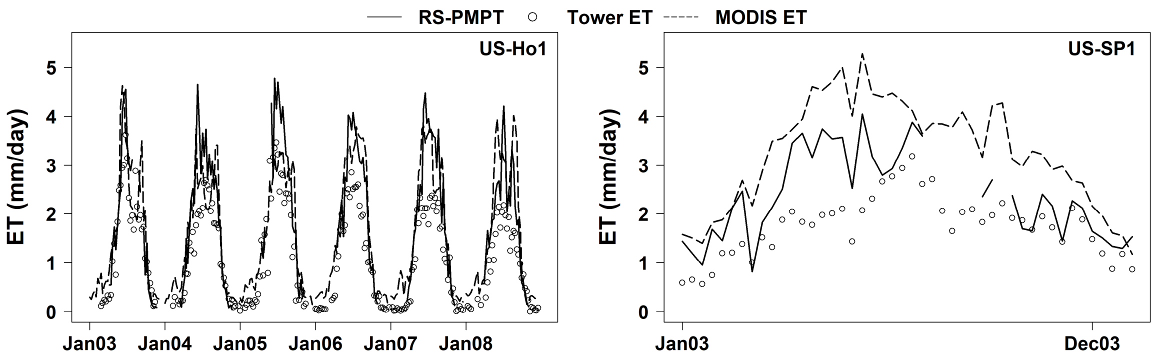

Figure 3. Seasonal time series of daily ET for the calibration evergreen forest sites either at eddy flux tower (open circle) or predicted by the MODIS (black line).

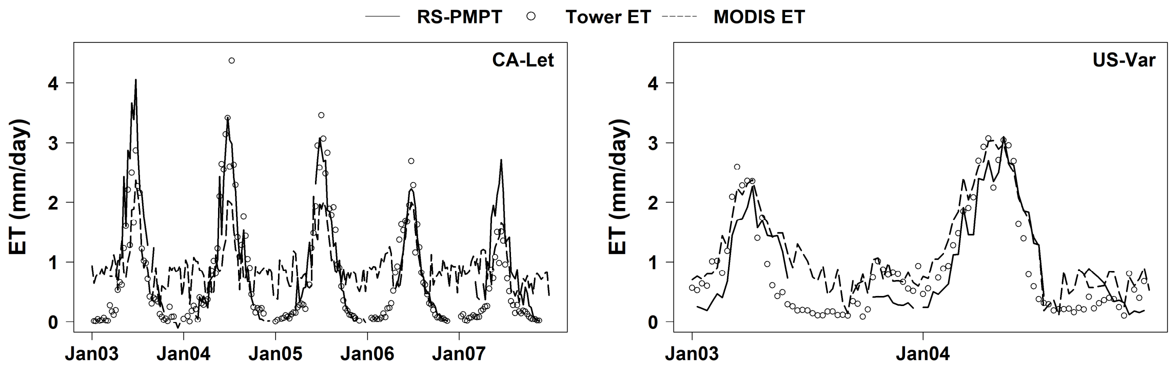

Figure 4. Seasonal time series of daily ET for the calibration grassland sites either at eddy flux tower (open circle) or predicted by the RS-ET model (black lines).

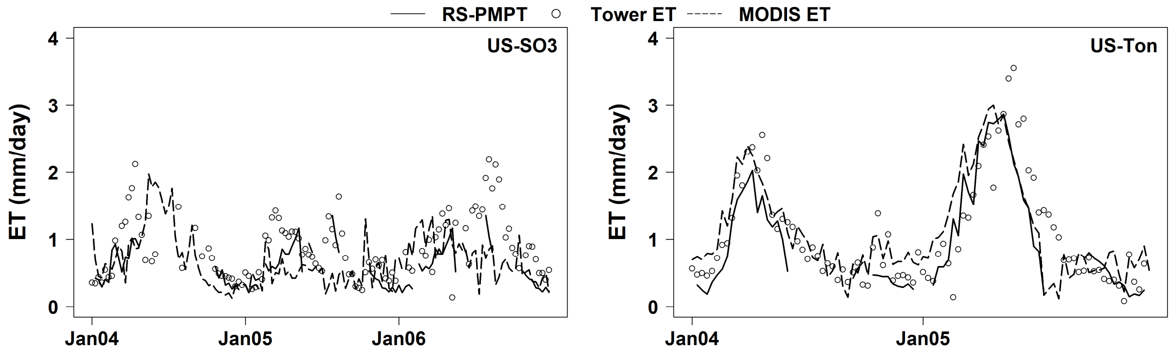

Figure 5. Seasonal time series of daily ET for the savanna and shrubland sites either at eddy flux tower (open circle) or predicted by the MODIS (black lines). "Missing RS-PMPT data for Sky Oaks are the result of missing satellite soil moisture data."

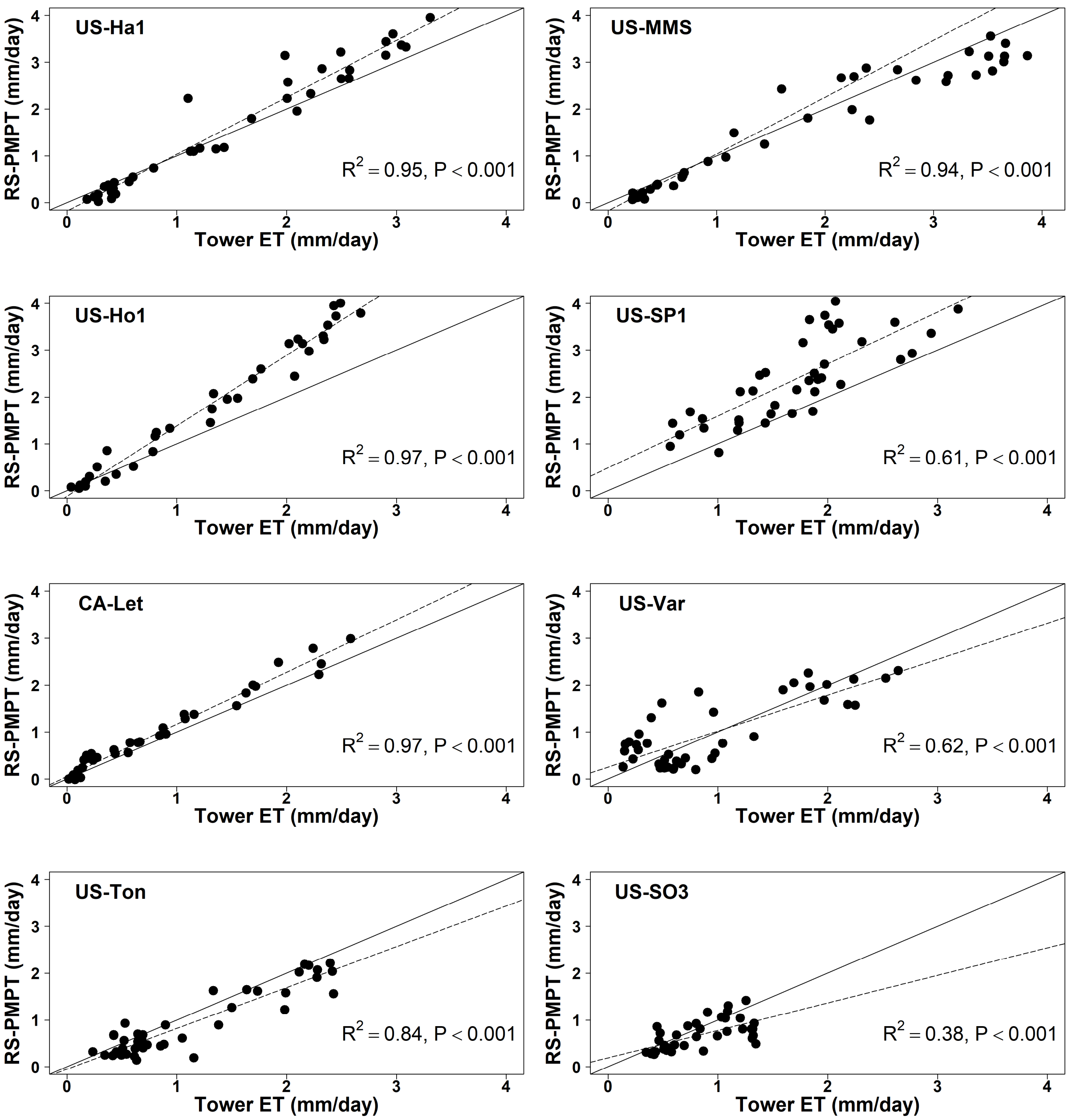

Figure 6. Average 8-day of the RS-PMPT ET estimates compared with average 8-day eddy flux tower ET for the calibration sites. The dashed line is the regression line and the black solid line is the 1:1 line. The data for each site represent the average 8-day data for the years included in the study (see Table 2)

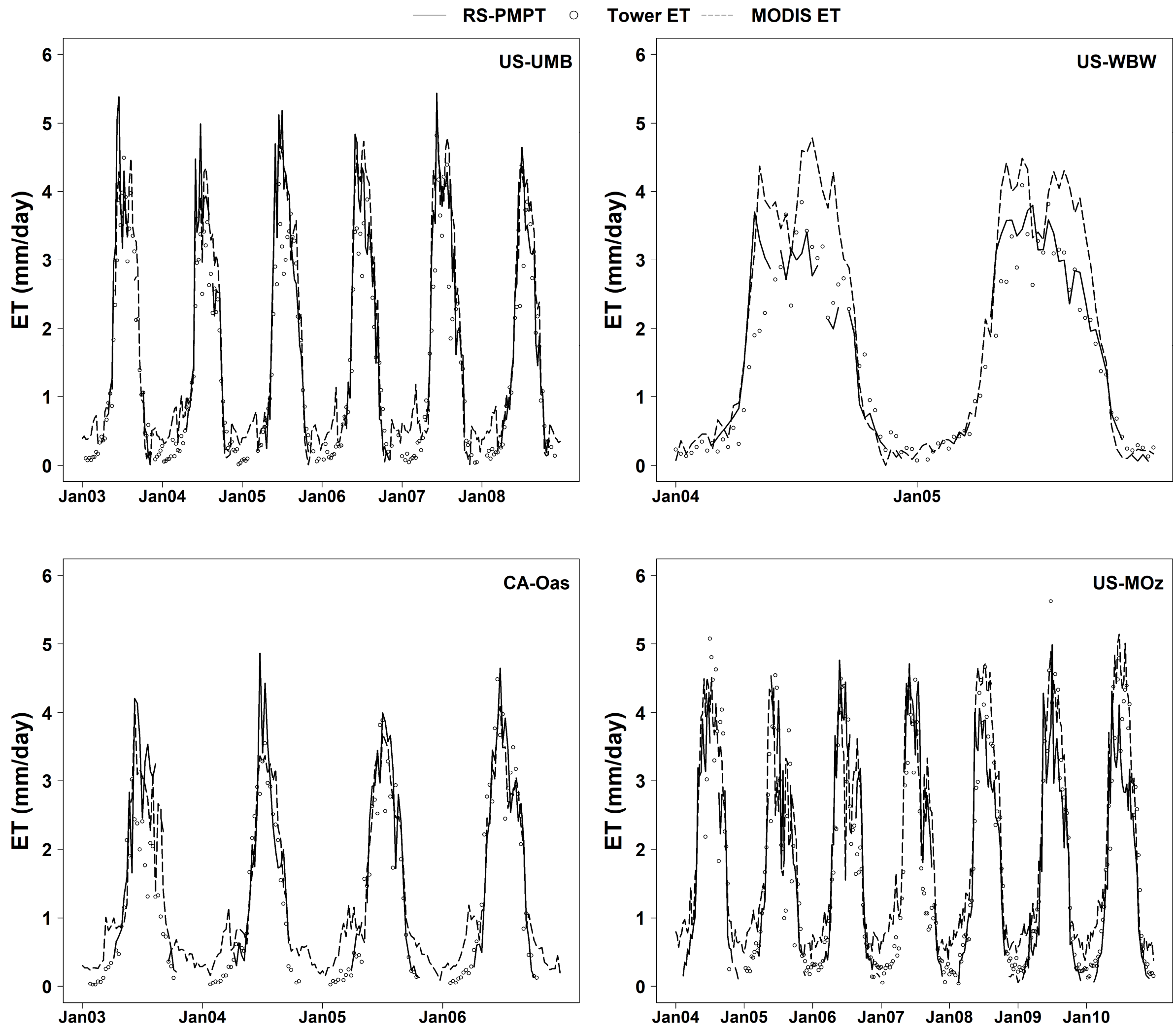

Figure 7. Seasonal time series of daily ET for the validation deciduous sites either at eddy flux tower (open circle) or predicted by the RS-ET model (black line).

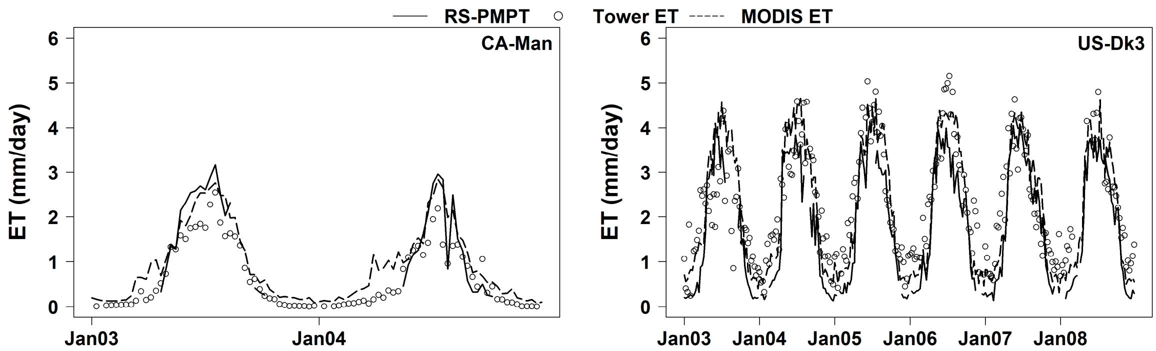

Figure 8. Seasonal time series of daily ET for the validation evergreen sites either at eddy flux tower (open circle) or predicted by the RS-ET model (black line).

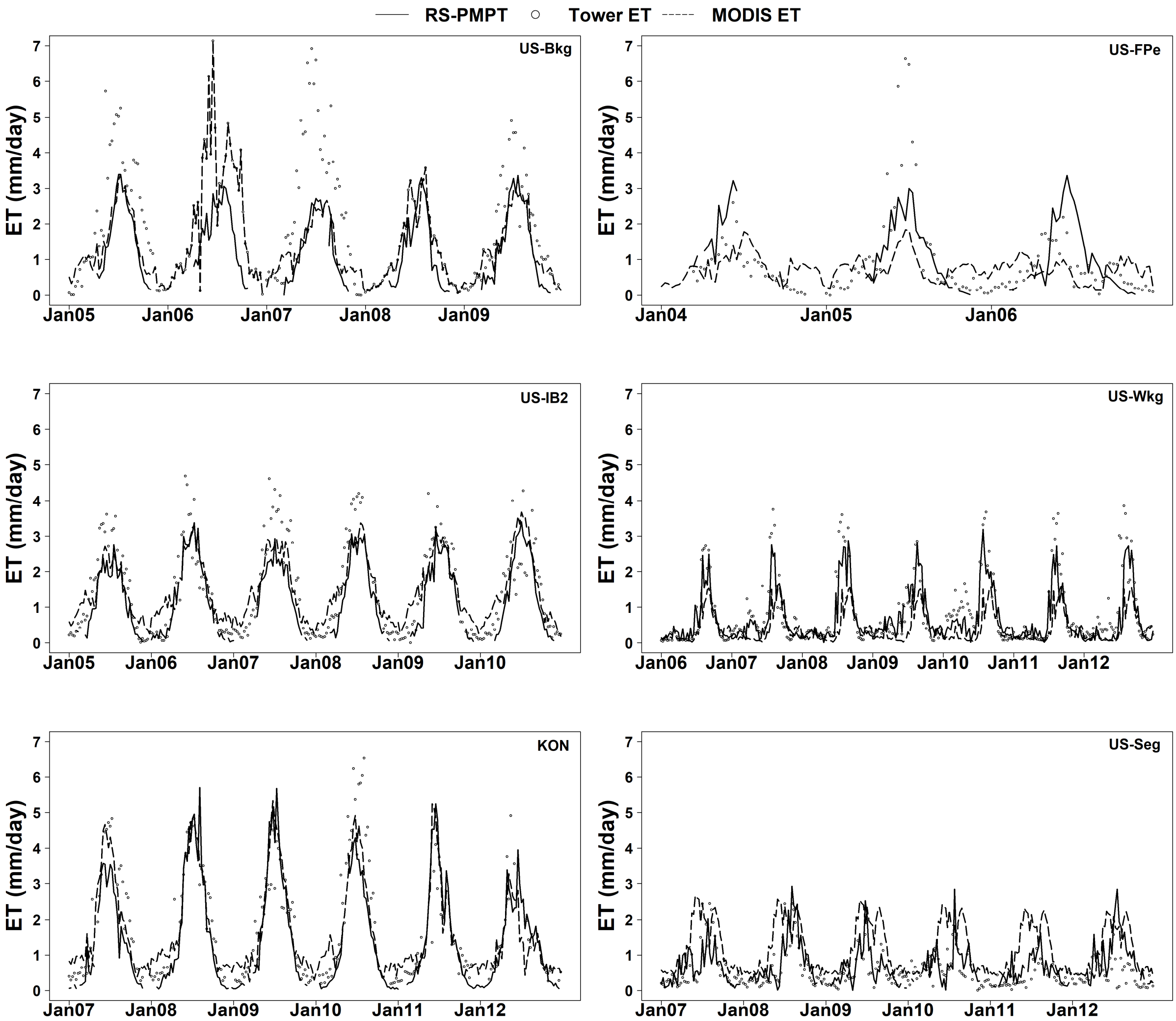

Figure 9. Seasonal time series of daily ET for the validation grassland sites either at eddy flux tower (open circle) or predicted by the RS-ET model (black line).

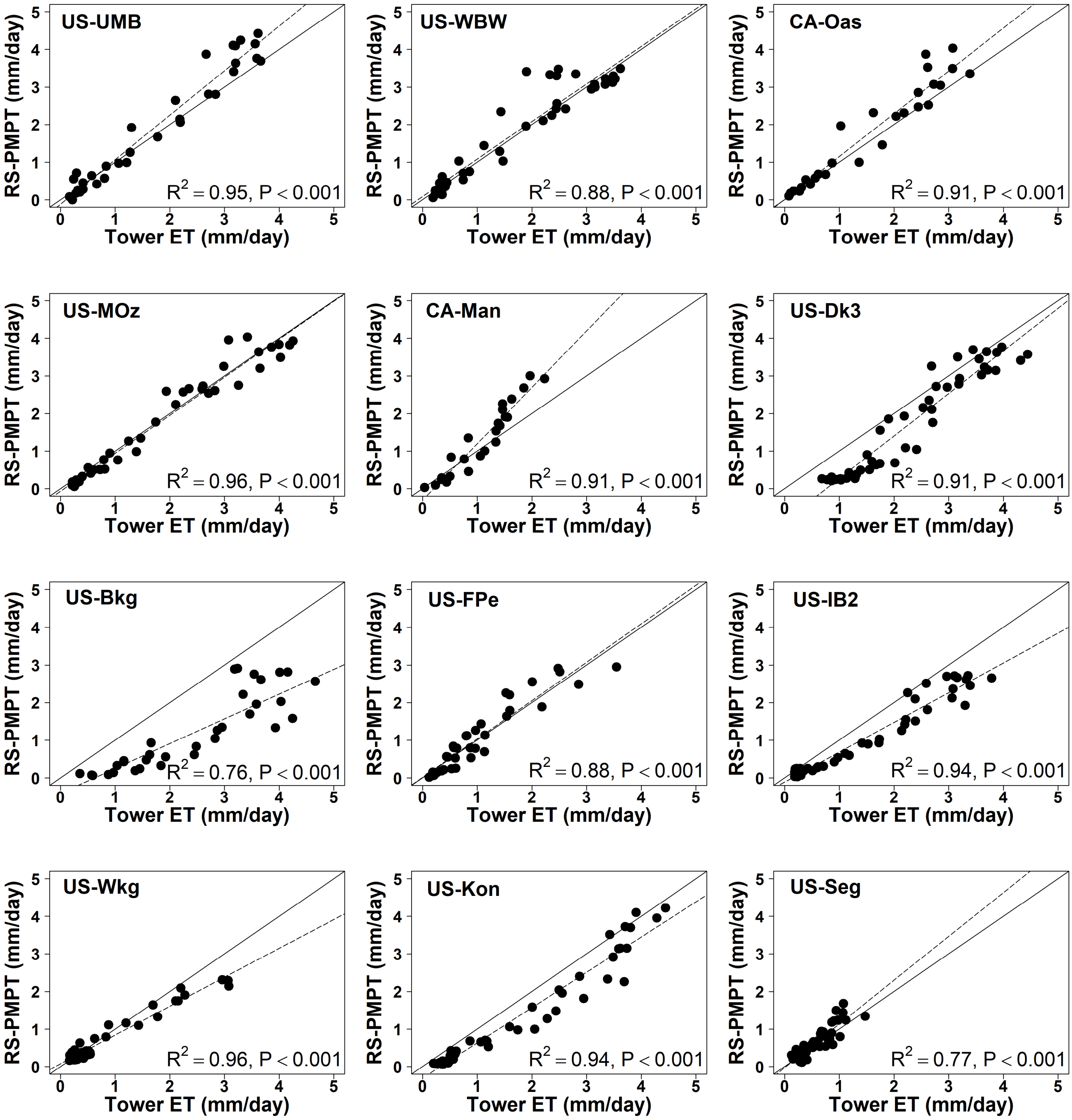

Figure 10. Average 8-day for the RS-PMPT ET estimates as compared to average 8-day eddy flux tower ET for the validation sites. The dashed line is the regression line and the black solid line is the 1:1 line. The data for each site represent the average 8-day data for the years included in the study (see Table 2)

Table 1. Model parameters, environmental constraints, and inputs for the RS-PMPT model.

Parameters	**Description:**	**Calibrated**	**Inputs**	**Reference**
R_{nc},; R_{ns} (W/m^2)	Net canopy radiation; net soil radiation	**-**	MODIS fpar version 005 (MOD 15A2 and MYD 15A2 layer name: Fpar_1km), CERES derived R_n (layer names: sfc_comp_sw-down_all_daily; sfc_comp_lw-down_all_daily; sfc_comp_sw-up_all_daily; sfc_comp_lw-up_all_daily)	Mu et al., 2011
f_{wet}	Wet surface fraction	-	MODIS LST version 005 (MOD11A2 and MYD11A2; layer names: LST_Day_1km and LST_Night_1km)	Fisher et al., 2008; Mu et al., 2011.
$f(T_s)$	Plant temperature constraint	Yes	MODIS LST	Gerosa et al., 2012
f(VPD)	Plant vapor pressure deficit constraint	Yes	MODIS LST	Mu et al., 2007; Hashimoto et al., 2008
$f(R_s)$	Plant solar radiation constraint	-	CERES derived R_n	Stewart, 1988; Dingman, 2002

f(θ)	Plant water constraint	-	CCI soil moisture (CCI SM v03.2, variable name: sm)	Stewart, 1988; Dingman, 2002
f_{SM}	Soil moisture constraint	-	MODIS albedo version 005 (MCD43A; variable names: shortwave_black and shortwave_white), MODIS LST	Garcia et al., 2013; Verstraeten et al., 2006
G (W/m^2)	Soil heat flux	-	MODIS LAI version 005 (MOD15A2 and MYD15A2; variable name: LAI_1km), CERES derived R_n	Kustas et al., 2003

1 Table 2. Ameriflux sites used for calibration and validation of the RS-PMPT model in this study.

Site Name	Vegetation Type	Climate	Longitude	Latitude	Year	Reference
			Calibration Sites			
Harvard Forest (US-Ha1)	Deciduous forest	Cold winter	72.17 W	42.54 N	2003-08	Goulden et al. (1996) http://dx.doi.org/10.17190/AMF/1246059
Morgan Monroe State Forest (US-MMS)	Deciduous forest	High summer rainfall	86.41 W	39.32 N	2003-08	Schmid et al. (2000) http://dx.doi.org/10.17190/AMF/1246080
Howland Forest (US-Ho1)	Evergreen forest	Cold winter	68.74 W	45.20 N	2003-08	Hollinger et al. (2005) http://dx.doi.org/10.17190/AMF/1246061
Austin Cary (US-SP1)	Evergreen forest	Hot summer	82.21 W	29.73 N	2003	Powell et al. (2008) http://dx.doi.org/10.17190/AMF/1246100
Tonzi Ranch (US-Ton)	Woody Savanna	Dry hot summer	120.96	38.43 N	2004-05	Xu and Baldocchi (2004) http://dx.doi.org/10.17190/AMF/1245971
Lethbridge (CA-Let)	Grassland	Warm summer	112.94 W	49.7 N	2003-07	Flanagan and Adkinson (2011) http://dx.doi.org/10.17190/AMF/1436318
Vaira Ranch (US-Var)	Grassland	Dry hot summer	120.95	38.40 N	2004-05	Xu and Baldocchi (2004) http://dx.doi.org/10.17190/AMF/1245984
Sky Oaks (US-SO3)	Shrubland	Dry hot summer	116.62 W	33.37 N	2004-06	Sims et al. (2006) http://dx.doi.org/10.17190/AMF/1246098
			Validation Sites			
Michigan Biological Station (US-UMB)	Deciduous forest	Cold winter	84.71W	45.56 N	2003-08	Schmid et al. (2003) http://dx.doi.org/10.17190/AMF/1246107
Walker Branch (US-WBW)	Deciduous forest	Hot summer	84.28 W	35.96 N	2004-05	Baldocchi (1997) http://dx.doi.org/10.17190/AMF/1246109
Southern Old Aspen (CA-Oas)	Boreal deciduous	Cool summer	106.19 W	53.63 N	2003-06	Barr et al. (2007) http://dx.doi.org/10.17190/AMF/1375197
Missouri Ozark (US-MOz)	Deciduous	Hot summer	92.2 W	38.74 N	2004-10	Gu et al. (2007) http://dx.doi.org/10.17190/AMF/1246081

Northern Old Black Spruce (CA-Man)	Boreal Evergreen	Cool summer	98.48 W	55.88 N	2003-04	Griffis et al., 2003 http://dx.doi.org/10.17190/AMF/1245997
Duke Loblolly Pine (US-Dk3)	Evergreen	Hot summer	79.09 W	35.97 N	2003-08	Katul et al. (1999) http://dx.doi.org/10.17190/AMF/1246048
Brookings (US-Bkg)	Grassland	Hot summer	96.83 W	44.34 N	2005-09	Meyers T.P http://dx.doi.org/10.17190/AMF/1246040
Fort Peck (US-FPe)	Grassland	Cold winter	105.1 W	48.3 N	2004-06	Meyers T.P http://dx.doi.org/10.17190/AMF/1246053
US-IB2	Grassland	Hot summer	88.24 W	41.84 N	2005-10	Matamala et al. (2008) http://dx.doi.org/10.17190/AMF/1246066
Walnut Gulch Kendall (US-Wkg)	Grassland	Dry cold steppe	109.94 W	31.73 N	2006-12	Scott (2010) http://dx.doi.org/10.17190/AMF/1246112
Konza Prairie (US-Kon)	Grassland	Hot summer	96.56 W	39.08 N	2007-12	Wilson et al. (2001) http://dx.doi.org/10.17190/AMF/1246068
Sevilleta (US-Seg)	Grassland	Dry cold steppe	106.7 W	34.36 N	2007-12	Anderson-Teixeira et al. (2011) http://dx.doi.org/10.17190/AMF/1246124

Table 3. Summary of the agreement analysis of RS-PMPT ET, MODIS ET, and tower ET.

		r^2	d	MAE (mm/d)	RMSE (mm/d)	MSE_s/MSE (%)	MSE_{us}/MSE (%)
Calibration Sites							
US-Ha1	RS-PMPT	0.95	0.90	0.18	0.34	26	74
	MODIS ET	0.92	0.55	0.84	1.21	79	21
US-MMS	RS-PMPT	0.94	0.89	0.27	0.36	38	62
	MODIS ET	0.96	0.77	0.56	0.62	82	18
US-Ho1	RS-PMPT	0.97	0.77	0.38	0.56	90	10
	MODIS ET	0.91	0.70	0.50	0.66	72	28
US-SP1	RS-PMPT	0.62	0.42	0.57	0.82	60	40
	MODIS ET	0.62	-0.34	1.50	1.69	84	16
US-Ton	RS-PMPT	0.84	0.80	0.24	0.34	37	63
	MODIS ET	0.72	0.75	0.30	0.37	13	87
CA-Let	RS-PMPT	0.97	0.88	0.15	0.21	59	41
	MODIS ET	0.66	0.58	0.49	0.58	83	17
US-Var	RS-PMPT	0.62	0.70	0.40	0.45	14	86
	MODIS ET	0.87	0.74	0.32	0.39	59	41
US-SO3	RS-PMPT	0.38	0.67	0.20	0.31	47	53
	MODIS ET	0.06	0.48	0.32	0.43	84	16
Validation Sites							
US-UMB	RS-PMPT	0.95	0.91	0.24	0.39	30	70
	MODIS ET	0.97	0.83	0.40	0.46	68	32
US-WBW	RS-PMPT	0.88	0.89	0.25	0.40	11	89
	MODIS ET	0.93	0.76	0.54	0.73	66	34
CA-Oas	RS-PMPT	0.92	0.90	0.22	0.37	24	72
	MODIS ET	0.94	0.83	0.28	0.42	71	29
US-MOz	RS-PMPT	0.96	0.91	0.21	0.30	11	89
	MODIS ET	0.96	0.84	0.39	0.45	62	38
CA-Man	RS-PMPT	0.91	0.83	0.36	0.46	67	33
	MODIS ET	0.93	0.73	0.31	0.40	70	30
US-Dk3	RS-PMPT	0.90	0.66	0.66	0.73	73	27

	MODIS ET	0.91	0.80	0.40	0.47	25	75
US-Bkg	RS-PMPT	0.76	0.65	0.94	1.44	90	10
	MODIS ET	0.72	0.69	0.81	1.13	86	14
US-FPe	RS-PMPT	0.88	0.85	0.21	0.41	61	39
	MODIS ET	0.43	0.58	0.60	0.79	94	6
US-IB2	RS-PMPT	0.95	0.80	0.44	0.55	84	16
	MODIS ET	0.91	0.82	0.39	0.46	67	33
US-Wkg	RS-PMPT	0.96	0.87	0.17	0.26	73	27
	MODIS ET	0.57	0.65	0.46	0.71	85	15
US-Kon	RS-PMPT	0.95	0.83	0.44	0.54	70	30
	MODIS ET	0.88	0.83	0.43	0.50	39	61
US-Seg	RS-PMPT	0.78	0.68	0.17	0.21	16	84
	MODIS ET	0.59	-0.08	0.59	0.76	66	34